N. Kusters, November 2020

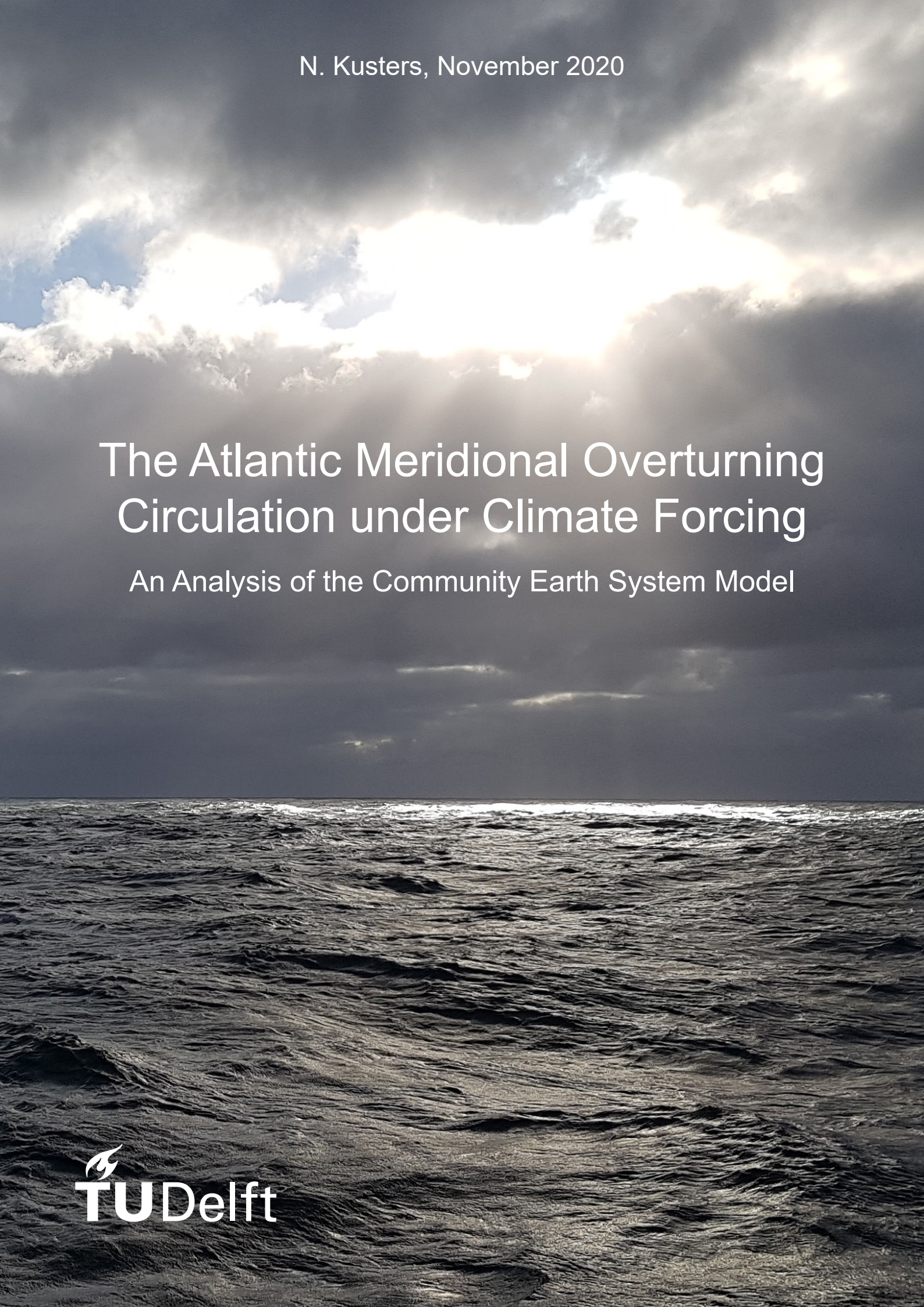

The Atlantic Meridional Overturning Circulation under Climate Forcing

An Analysis of the Community Earth System Model

TU Delft

The Atlantic Meridional Overturning Circulation under Climate Forcing

An Analysis of the Community Earth System Model

by

N. Kusters

to obtain the degree of Master of Science
at the Delft University of Technology,
to be defended publicly on Friday 13 November 2020 at 11:45 AM.

Student number:	4301676	
Thesis committee:	Dr. C. A. Katsman,	TU Delft, supervisor
	Prof. Dr. J. Pietrzak,	TU Delft
	Dr. M. Petrini,	TU Delft
	Dr. M. Vizcaino,	TU Delft

An electronic version of this thesis is available at `http://repository.tudelft.nl/`.

Cover photo: Irminger Sea on the 1^{st} of August, 2020. Photo by Niek Kusters.

TU Delft

Preface

This thesis reports on my graduation work for the MSc. Civil Engineering at TU Delft. From this master program, I have completed the Hydraulic Engineering track. It also marks the end of my time spent as a student in Delft.

A lesson I have learned during this summer is that you can plan as much as you want, but it will always go a different way. Who could have foreseen, almost ten months ago, what challenges needed to be overcome before the final result of this thesis could be presented? A global pandemic made that most of the work for this thesis was carried out from home, instead of time spent in an office at the university.

The pandemic caused not only negative challenges, it also opened up the opportunity to join a research cruise from the Royal Netherlands Institute for Sea Research (NIOZ) to the Irminger Sea. Although the data was not used for this thesis, I have learned a lot during the cruise on oceanography and doing fieldwork. It was a true adventure! Femke, Fleur, Elodie, Nora and Rick, thank you for the amazing time in our corona-free bubble on the Atlantic Ocean!

A lot of people supported me during the writing of this thesis. First, I would like to thank Dr. Caroline Katsman, Thank you for all our meetings during which we had good conversations and discussions. I have learned a lot from these discussions and appreciate it very much. Also thanks for all the feedback and proofreading of report. It definitely improved the final product. Second, I would also like to thank the rest of the committee; Prof.Dr. Julie Pietrzak, Dr. Michele Petrini and Dr. Miren Vizcaino. Thank you for the valuable comments and remarks during the writing of this thesis.

Furthermore, I am grateful for all the people I have met during my time as a student, both in Delft and abroad. You all made that my student years were such an awesome time. A special note to Koen, I enjoyed our coffee breaks when we were studying from home during the corona-pandemic. These coffee breaks helped in keeping me focused and our discussions gave valuable improvements for my thesis.

Of course, I also have to thank my parents and brother. Thank you for all the encouragement and support during the time I spent in Delft and when I was abroad.

Before you lies my thesis, the final product of this project. Wishing you a pleasant reading.

Niek Kusters
Delft, November 2020

Abstract

The Atlantic Meridional Overturning Circulation (AMOC) is a key component in the Earth System. Given its important role in the climate system, variability in the AMOC strength is expected to have great impact on the global climate. The current observational timeseries are not long enough to make climate projections for the end of the century or even longer. Therefore, coupled climate models play an important role in the making of end of century climate projections on the AMOC strength.

A known issue with the current generation of global coupled climate models is that the grid resolution is generally too coarse to resolve smaller scale processes such as mesoscale eddies. Observations and modelling studies suggest that mesoscale eddies play an important role in the exchange of water between convection regions and downwelling regions. When such processes are absent or parametrized incorrectly, it can have an influence on the climate projections based on these model simulations.

This study analysed the AMOC characteristics in two different simulations of the Community Earth System Model; a reference simulation (referred to as piControl) and a simulation in which the atmospheric CO_2 concentrations have been increased to four times the initial concentration (referred to as 1pctCO2).

First, the AMOC characteristics in the piControl simulation are analysed using both a Eulerian and a Lagrangian approach. The Eulerian analysis shows that deep mixed layers, an indicator for convection, are present in the subpolar North Atlantic. Compared to observations and higher-resolution ocean-only models are these located closer to the West-Greenland coast. Strong vertical velocities are found over the continental slopes, especially over the steep continental slopes around Greenland.

Second, the Lagrangian analysis showed the consequences of the coarse grid in the model. Only a single pathway around the subpolar gyre was observed. This implies that particles will experience convection while crossing the interior of the Labrador Sea, but only will experience downwelling when their individual pathway comes close enough to the continental slopes around Greenland. Furthermore, there is only limited exchange of particles with the regions north and south of the subpolar gyre. In the export of deep waters to the subtropical gyre, does it seem that the particles are being blocked by the North Atlantic Current.

Third, the changes in the AMOC characteristics in the 1pctCO2 simulation are compared to the piControl simulation. In the 1pctCO2 simulation have deep mixed layers disappeared from the subpolar North Atlantic and convection in this region has shut down. A new fresh(er) surface layer in the Labrador Sea has intensified the stratification and prohibits the formation of deep mixed layers. Instead of the deep mixed layers in the subpolar North Atlantic have new deep mixed layers emerged between 30° N and 40° N. In general are velocities reduced in magnitude in the 1pctCO2 simulation, but the stronger vertical velocities can still be found over the continental slopes.

In conclusion, the results show that the CESM model can reproduce the two components of the AMOC reasonably well, but the connection in the form of mesoscale eddies is missing. This illustrates that a overturning streamfunction simplifies the complexity of the overturning process. The overturning streamfunction is a measure for the overturning strength, but it does not take into account how and if the convection process and the exchange between convection and downwelling are represented.

Key words: AMOC, Climate change, CESM, Lagrangian analysis, Climate projections, coupled model, mixed layer depth

Contents

Preface iii

Abstract v

Contents vii

List of Acronyms ix

List of Figures xi

1 Introduction 1

2 Scientific background 3
- 2.1 The Atlantic Meridional Overturning Circulation . . . 3
- 2.2 Convection in the subpolar North Atlantic . . . 5
- 2.3 The different watermasses of the AMOC . . . 6
- 2.4 Ocean Modelling . . . 7
- 2.5 Problem definition and objective . . . 8

3 Specifications of the Community Earth System Model and OceanParcels 9
- 3.1 The Community Earth System Model . . . 9
  - 3.1.1 POP2 Specifications . . . 10
  - 3.1.2 Simulations and available data . . . 11
- 3.2 Lagrangian methods . . . 12
- 3.3 OceanParcels and its use in a coarse model . . . 13
- 3.4 Summary . . . 14

4 Research approach 15
- 4.1 Eulerian approach . . . 15
- 4.2 Lagrangian approach . . . 15
  - 4.2.1 Location . . . 17
  - 4.2.2 Time . . . 17
  - 4.2.3 Number of particles . . . 17
  - 4.2.4 Summary of the total particleset . . . 18

5 Analysing the piControl simulation 19
- 5.1 Eulerian analysis . . . 19
  - 5.1.1 Mixed Layers in the northern Atlantic Ocean . . . 19
  - 5.1.2 Overturning in depthspace, vertical velocities . . . 21
- 5.2 Lagrangian analysis . . . 22
  - 5.2.1 Particle pathways in the subpolar gyre . . . 22
  - 5.2.2 Example of a particle experiencing overturning in density space . . . 24
  - 5.2.3 Example of a particle experiencing overturning in depth space . . . 26
- 5.3 Summary . . . 28

6 Analysing the 1pctCO2 simulation 29
- 6.1 Mixed layers and vertical velocities in the 1pctCO2 simulation . . . 29
- 6.2 Changes between the 1pctCO2 and piControl simulations . . . 32
- 6.3 Summary . . . 35

7 Conclusion and discussion 37

8 Recommendations 41

Bibliography 43

List of Acronyms

AMOC	Atlantic Meridional Overturning Circulation
CAM	Community Atmosphere Model
CESM	Community Earth System Model
CISM	Community Ice Sheet Model
CLM	Community Land Model
CMIP	Coupled Model Intercomparison Project
DSOW	Denmark Strait Overflow Water
DWBC	Deep Western Boundary Current
IC	Irminger Current
IPCC	Intergovernmental Panel on Climate Change
ISOW	Iceland Scotland Overflow Water
LSW	Labrador Sea Water
NAC	North Atlantic Current
NADW	North Atlantic Deep Water
Parcels	Lagrangian particle tracking software OceanParcels
POP	Parallel Ocean Program
piControl	Pre-Industrial Control simulation
1pctCO2	Simulation with an increase of 1% in the CO_2 concentration

List of Figures

2.1 A schematic overview of the thermohaline circulation. Surface currents are red, deep currents are blue. (From Bollmann et al. (2010), their Figure 1.8) 4
2.2 Projections for the AMOC strength in Sverdrups (1 $Sv = 10^6\ m^3/s$) by different climate models in the RCP8.5 scenario of the IPCC (Adapted from Collins et al., 2013, their Figure 12.35) 4
2.3 Density along the World Ocean Circulation Experiment (WOCE) AR7W section in the Labrador Sea of (a) October '96 and (b) March '97, based on field measurements (From Pickart et al., 2002, their Figure 8c) 5
2.4 Currents in the subpolar North Atlantic (From Morozov et al., 2010, their Figure 2.6) 6

3.1 Flowchart of the data with CESM and OceanParcels. 9
3.2 Illustrations of the curvilinear staggered B-grid. (a) shows an example of a grid cell, with the velocity and tracer points indicated. (b) shows the displacement of the grid northpole to the north of Greenland. 10
3.3 Sea Surface Temperature in two POP simulations on (a) a 1° grid and (b) a 0.1° grid. (Courtesy of Prof. H.A. Dijkstra, Utrecht University) 11
3.4 Strength of the North Atlantic Meridional Overturning Circulation Index (in Sv, black) and the local maximum mean January-Februari-March mixed layer depth within four regions: Labrador Sea (red), Irminger Sea (purple), Iceland Basin (green) and Barent Sea (blue). Dashed lines represent pre-industrial conditions (From Muntjewerf et al., 2020, their Figure 3.a) 12
3.5 Example of backward computing of a parcel trajectory, showing the first five timesteps of a parcel in the piControl simulation 13

4.1 Mean Meridional Streamfunction of the northern Atlantic Ocean, averaged over 20-year periods in different periods of the simulation. The streamfunction of the piControl simulation can be found in the upper panel, the lower two panels belong to the 1pctCO2 simulation (From Muntjewerf et al., 2020, their Figure 3.b) 16
4.2 Cross-section at $54.75°N$ of the meridional velocity in the first month of (a) the piControl simulation and (b) a map of the starting location. The particles are being released between the two red lines. 16
4.3 An overview of the distribution of the particleset at the starting location of the simulation. 18

5.1 Mixed layer depth in the northern Atlantic Ocean in March (month 3 of the dataset) 20
5.2 Vertical velocities in March (month 3 of the dataset), the 1000m mixed layer depth contour is indicated in green 20
5.3 Cross-sections of the vertical velocities at (a) $54.75°N$ and (b) $61.75°N$, with the mixed layer depth indicated in black 21
5.4 Variability of the vertical velocity over time at (51.25W, 61.75N) 22
5.5 Trajectories for a selection of 491 particles. The particles are traced backwards in time for a duration of 15 years. The starting location is marked in red. 23
5.6 Trajectories of 2530 particles. The particles are traced forwards in time for a duration of 10 years. The starting location is marked in red. The trajectories of ExportSouth are marked in orange. . . . 23
5.7 Example trajectory illustrating overturning in density space. The depth anomaly compared to the particle depth at $54,75°\ N$ is plotted in (a), in (b) the density anomaly compared to the particle density at $54,75°\ N$ is plotted. (c) showsthe particles temperature, salinity and density over time as well as the depth (all in blue). The bottom panel of (c) also shows the local mixed layer depth marked in orange. 25
5.8 The change in depth versus the change in density between $40°W$ and $54.75°N$. The colors mark the particle depth at $54.75°N$. 26

5.9 Example trajectory of overturning in depth space. The depth anomaly compared to the simulation start is plotted in (a), in (b) the density anomaly compared to the simulation start is plotted. (c) shows temperature, salinity and density over time as well as the depth together with the local mixed layer depth. 27

6.1 Mixed Layer Depths north of the equator for the 1pctCO2 simulation. The frame marks the area over which the maximum mixed layer in the Labrador Sea has been determined. 30
6.2 Cross-section of the meridional velocities at $54,75°\ N$, during January in the 1pctCO2 simulation 30
6.3 Vertical velocities at 500 meter depth in the 1pctCO2 simulation, with the 500m contour of the mixed layers indicated in green. 31
6.4 Cross-sections of the vertical velocities at (a) $54.75°N$ and (b) $61.75°N$, with the mixed layer depth indicated in black. Please note the scale differences compared to Figure 5.3 31
6.5 The differences between the 1pctCO2 simulation and the piControl simulation for (a) temperature, (b) salinity and (c) density. The cross-sections are taken at $55°W$. The frame in the figures marks the Labrador Sea. 33
6.6 The near-surface temperature anomaly in Kelvin between model years 331-350 of the 1pctCO2 simulation and the piControl simulation (From Muntjewerf et al., 2020, their Figure 1.d). 33
6.7 Variability of (a) temperature, (b) salinity and (c) density over time at (73.75W,36.75N) in the 1pctCO2 simulation. The local mixed layer depth is indicated by the black line. 34

1

Introduction

The oceans play an important role in the climate system. The oceans have been estimated to have taken up more than 90% of the excess heat in the climate system since 1970's and between 20-30% of the (total) anthropogenic CO_2 production since the 1980's (IPCC, 2019). With the changing climate, the ocean and ocean circulation are experiencing unseen changes. The Atlantic Meridional Overturning (AMOC) is a key component in the Earth System. The AMOC transports heat and salt from the lower latitudes to the higher latitudes in the Atlantic Ocean. Warm and salty surface waters flow to the higher latitudes, after which transformed cold and fresh(er) deep waters return south.

Field observations from cross-basin mooring-arrays show that the AMOC has variability on all accessible timescales (de Jong and de Steur, 2016; Smeed et al., 2014). The variability on the longer (multi-decadal) timescales is linked to the sea surface temperature and to weather and climate variability across the globe; rainfall in South America, Africa and Asia, hurricane activity over the Atlantic Ocean, Arctic sea-ice coverage, the climate in Europe and North America and to variability in the ocean carbon cycle (Lozier et al., 2017; McCarthy et al., 2017).

Given its important role in the climate system, variability in the AMOC strength is expected to have great impact on the global climate. IPCC (2019) projects with high confidence that the AMOC strength will weaken under climate change. Given the absence of observational timeseries long enough to make climate projections for the end of the century and even longer, the projections of the IPCC (2019) are based on an ensemble of climate model projections participating in the Coupled Model Intercomparison Project (CMIP). One of the models participating in CMIP is the Community Earth System Model (CESM). The model that will be used in this study is the CESM model. Under climate forcing, also the CESM model does show a decline in the AMOC strength.

A known issue with the current generation of global coupled climate models is that the grid resolution is generally too coarse to resolve smaller scale processes such as mesoscale eddies. Observations (e.g. De Jong et al., 2018), idealized model studies (e.g. Georgiou et al., 2020b) and higher resolution ocean (only) models (e.g. Sayol et al., 2019) suggest that mesoscale eddies play an important role in the exchange of water between convection regions and downwelling regions. When such processes are absent or parametrized incorrectly, it can have an influence on the climate projections based on these model simulations.

The AMOC and its variability can be looked at from two perspectives, a Eulerian perspective, with a fixed frame of reference, and a Lagrangian perspective, with a moving frame of reference. While a Eulerian approach, such as observations, is important to get a better understanding of for example the AMOC variability or the formation of deep water, a Lagrangian approach gives insight in the three dimensional structure and in the pathways of the water masses (Bower et al., 2019).

To improve the predictions on climate change, which are made using the predictions from climate models, an improved knowledge on the key elements in the climate system is needed. This study aims to improve the current understanding of the behaviour of the AMOC in the CESM model, using both a Eulerian as well as a Lagrangian perspective.

In the rest of this report, Chapter 2 will treat the relevant concepts more thoroughly. The chapter will be concluded with the formulation of the research questions. With the research questions formulated, Chapter 3 will discuss the used models and the available data. In Chapter 4, the approach to this research will be outlined. Following this approach, Chapter 5 will discuss the analysis of the so-called piControl simulation. Chapter 6 will discuss the analysis of the model after the increase of the atmospheric greenhouse gases. Chapter 7 will discuss the results of Chapter 5 and 6 and formulate conclusions. Recommendations for further research are given in Chapter 8.

2

Scientific background

This chapter will introduce the main concepts needed to understand the functioning of the AMOC and how it can be represented in climate models. The first section explains the functioning of the AMOC and its role in the climate system. Section 2.2 introduces the topic of deep convection, followed in Section 2.3 by an introduction of the different water masses that are part of the AMOC. Section 2.4 outlines why there is the need for ocean modelling and a few of the advantages and disadvantages. The chapter is concluded with the formulation of the main research question and several subquestions.

2.1. The Atlantic Meridional Overturning Circulation

The oceans play an important role in the climate system. The oceans have been estimated to have taken up more than 90% of the excess heat in the climate system since the 1970's and between 20-30% of the (total) anthropogenic CO_2 production since the 1980's (IPCC, 2019). With the changing climate, the ocean and ocean circulations are experiencing unseen changes.

Heat and salt are being distributed across the globe by various circulations. One of these circulations is described as the Global Conveyor belt (Broecker, 1991) or the thermohaline circulation. A schematic overview of the thermohaline circulation is added in Figure 2.1. The global conveyor belt transports heat and salt across the globe. In general the global conveyor belt transports warm waters across the surface and colder waters in the deep ocean. For a large part, there is only little exchange between the surface part of the conveyor belt and the deep part, since the oceans are (strongly) stratified. Only in a few locations (the yellow dots in Figure 2.1), the connection is made and is there a connection between the warm surface water and the cold deep waters. In the subpolar North Atlantic Ocean is this connection made by the Atlantic Meridional Overturning Circulation.

The exchange between the warm surface currents and the cold deep currents is described by the Atlantic Meridional Overturning Circulation (AMOC). Warm water is transported across the surface northwards by the Gulf Stream. In the marginal seas of the subpolar North Atlantic Ocean, the Labrador, Irminger and Nordic Seas, the water is cooled by the cold atmosphere. This strong cooling of the water has the potential to increase the density of the watermasses to such extend that they can sink to the deep ocean. From there, the lower limb of the AMOC flows southwards towards the Southern Ocean.

The heat that is released by the ocean is important for maintaining the relatively mild climate that we know in western Europe, compared to similar latitudes across the ocean (McCarthy et al., 2017). Under climate change, it is with high confidence that the AMOC is expected to weaken in strength (IPCC, 2019). Figure 2.2 shows the projections of the AMOC strength for an ensemble of climate models for the RCP8.5 scenario (RCP stands for Representative Concentration Pathway, 8.5 is the amount of extra radiative forcing kept within the Earth System by 2100, in $[W/m^2]$). A weakening of the AMOC is expected to have a great impact on the global climate. Drier summers, more storms in northwestern Europe and sea level rise are expected to be among the effects (IPCC, 2019; McCarthy et al., 2017).

The strength of the AMOC displays a strong variability (Collins et al., 2013; de Jong and de Steur, 2016). The AMOC strength changes on all timescales; seasonal, annual, decadal and longer. But these regions of the planet,

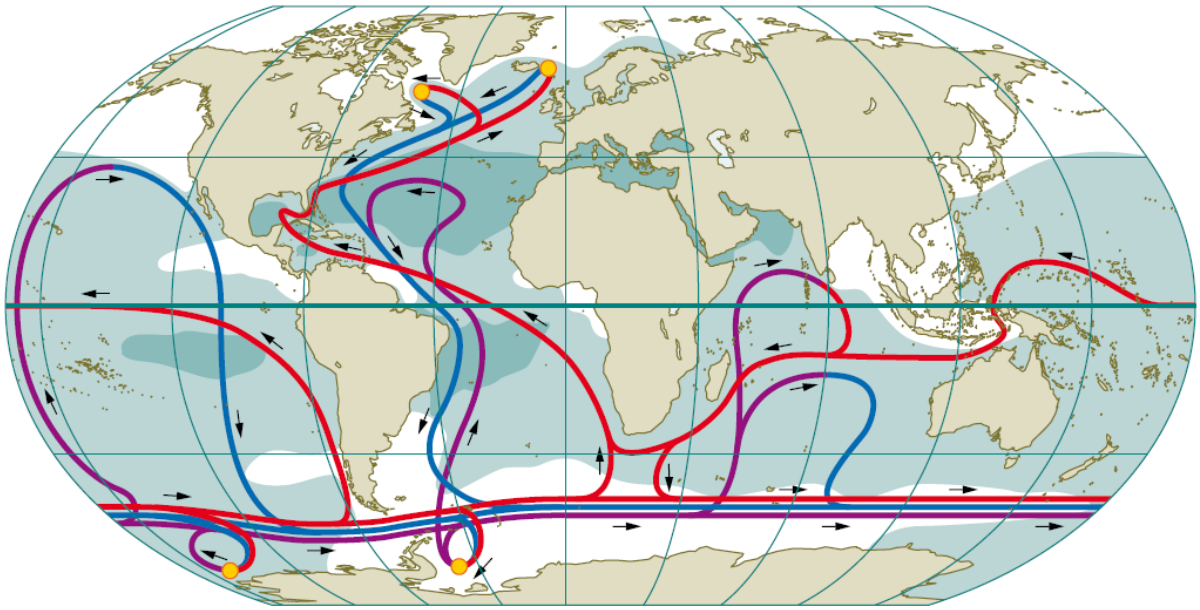

Figure 2.1: A schematic overview of the thermohaline circulation. Surface currents are red, deep currents are blue. (From Bollmann et al. (2010), their Figure 1.8)

where the surface flow is connected to the deep flow, are also very remote and conditions are harsh, which makes field measurements difficult to obtain. Since 2004 in-situ measurements of the AMOC strength are being made at the RAPID-MOCHA array (at 26.5° N) (Smeed et al., 2014) and since 2014 by the OSNAP array (between New Foundland, Canada - Cape Farewell, Greenland - Scotland) (Lozier et al., 2017). These measurements, together with modelling studies are used to get a better understanding of the variability of the AMOC and for future predictions on how the AMOC will change under climate change.

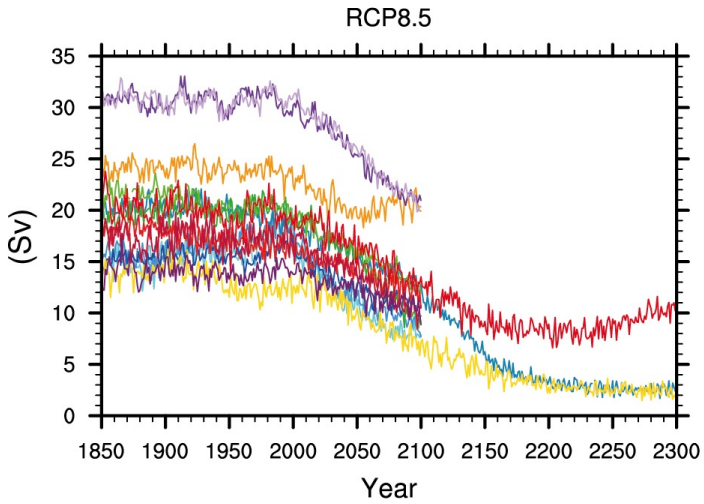

Figure 2.2: Projections for the AMOC strength in Sverdrups (1 $Sv = 10^6\ m^3/s$) by different climate models in the RCP8.5 scenario of the IPCC (Adapted from Collins et al., 2013, their Figure 12.35)

2.2. Convection in the subpolar North Atlantic

The yellow dots in Figure 2.1 mark the locations where the connection is made between warm surface waters and the cold deep waters. Elsewhere, usually the oceans are stratified and there is little vertical mixing. In the stratified state the densest water can be found at the bottom and the density decreases when you move up through the water column. As an example, Figure 2.3a shows field measurements across the Labrador Sea during a cruise in October. The figure shows the sigma ($\sigma = \rho - 1000$ [kg/m^3]), with the densest waters at the bottom, and decreasing density higher up.

The density of water is determined by an equation of state, relating density to the observed temperature and salinity of the water.

A consequence of the stratification is that before the northward flowing waters at the surface can be overturned to become the southward flowing deep waters, an increase in the density of the watermass is needed. This process in which the properties of the watermasses are changed is called (deep) convection. This convection happens in the subpolar North Atlantic Ocean through severe cooling of the water by the atmosphere. In the winter months (February, March), the cooling is strong enough for convection to happen.

As the surface layers of the water become colder as they lose their heat to the atmosphere, they also become denser. At some point, the surface layers become denser than the water layers below, the stratification collapses and the watercolumn mixes vertically from the surface, to the depth at which the density starts to increase again. In this situation the density is uniform through the watercolumn, from the surface to the mixing depth. Figure 2.3b shows field measurements at the same cross-section of the Labrador Sea during active convection. The figure clearly shows the mixed waters, with a uniform density extending to a depth of approximately 1000 meter.

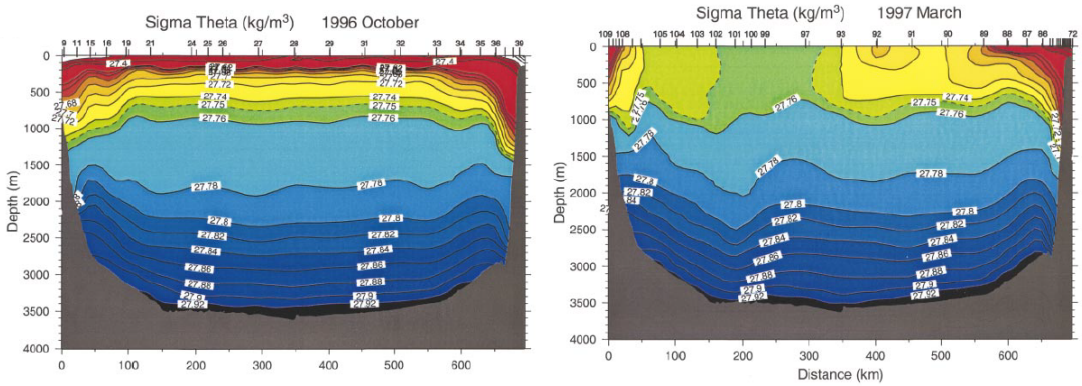

(a) (b)

Figure 2.3: Density along the World Ocean Circulation Experiment (WOCE) AR7W section in the Labrador Sea of (a) October '96 and (b) March '97, based on field measurements (From Pickart et al., 2002, their Figure 8c)

The mixed layer depth indicates the depth to which the convection process reaches, or in other words, the thickness of the layer with the uniform density. The depth of the mixed layer is not constant, it is time dependent, as the mixed layers need time to develop, and it is determined by the conditions of the atmosphere. In harsh winters, the mixed layer depth is larger than in mild winters. Besides the conditions of the current winter, also the conditions in the previous winters have an influence on how deep the convection process reaches. Several harsh winters in a row will have a positive effect on the mixed layer depth.

During convection, the water is completely mixed, but in order for the overturning to be complete, the convected waters need to sink to greater depths. In the Labrador Sea, the deepest mixed layers can be found in the interior of the sea, as can be seen in Figure 2.3b. However, conceptual modelling studies (Georgiou et al., 2020b; Sayol et al., 2019; Straneo, 2006) have shown that convection occurs in the interior of the sea, while the downwelling occurs in the boundary current, which can be found over the steep continental slope around the edges of the sea. The strongest downwelling can be found in the region near the west coast of Greenland (Georgiou et al., 2019; Katsman et al., 2018). So a mechanism is needed to bring the water out of the interior to the boundary current. If such a mechanism is not present, the consequence would be that a stagnant pool of dense water will form in the interior of the Labrador Sea. From modelling studies we know that eddies play a major role in the exchange between the interior and the boundary current. The eddies are being shed from the

West Greenland Current over the steep bathymetry on the western side of Greenland, near Cape Farewell. There are different pathways, with different timescales, that the water can take in the exchange between the interior and the boundary current, before it is being exported out of the Labrador Sea (Georgiou et al., 2020b). Some convection might also happen in the boundary current, so this water does not leave the boundary current. Another part of the water from the interior can join the boundary current directly near the Labrador coast. The last possible pathway is for the water to be transported back to the West-Greenland coast and flow with the boundary current around the Labrador Sea (Georgiou et al., 2020a).

2.3. The different watermasses of the AMOC

The general idea of the AMOC becomes clear from the sections above. There is the 'upper limb', transporting warm water northwards at the surface and the 'lower limb', transporting the cold, deep water southwards in the deep ocean. The connection between these two limbs is being made by deep convection, which happens in the marginal seas of the subpolar North Atlantic; the Labrador, Irminger and Nordic Seas. However, Figure 2.1 is a oversimplification of reality. In reality, the ocean currents form a complex system of many different, meandering, recirculating currents.

The upper limb of the AMOC is formed by the North Atlantic Current (NAC). The NAC follows the American coastline up to the region south of Newfoundland. South of Newfoundland it leaves the shelf behind and starts to cross the ocean in the direction of Ireland and the UK. Over the Mid-Atlantic Ridge, a part of the NAC branches of to the north, to continue as the Irminger Current (IC). The IC flows counterclockwise around the Irminger Basin, before it flows around Greenland into the Labrador Sea. The other part of the NAC continues through the Iceland Basin, over the Greenland-Scotland Ridge, into the Norwegian Sea. The NAC continues all the way along the Norwegian coast towards the Barents Sea.

When the water leaves the mixed layer during the convection process, its properties in terms of temperature, salinity and density are being conserved. Below the mixed layer, mixing occurs mainly along isopycnals (Brüggemann and Katsman, 2019). This allows to trace the deep waters back to its region of origin.

The entire product of the different convection sites is called North Atlantic Deep Water (NADW). The NADW can be found all the way to the southern Atlantic Ocean (Bullister et al., 2013).

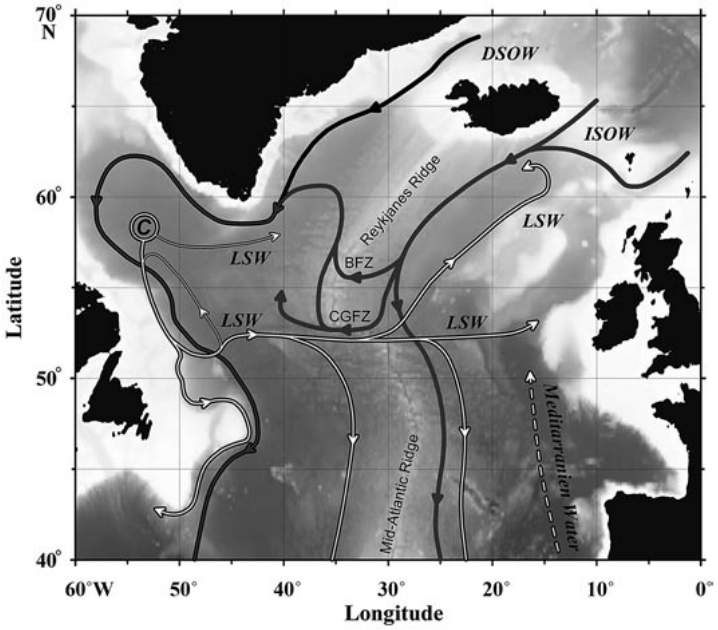

Figure 2.4: Currents in the subpolar North Atlantic (From Morozov et al., 2010, their Figure 2.6)

Figure 2.4 shows the watermasses of the lower limb of the AMOC. The deep water from the Nordic Seas flows southwards over two sills. The first watermass is the Iceland-Scotland-Overflow-Water (ISOW) which flows

from the Norwegian Sea into the Iceland Basin through the Faeroe Channel. Part of it flows south on the eastern side of the Mid-Atlantic Ridge. The other part flows southwards on the eastern side of Reykjanes Ridge, crosses the Ridge through two deeper parts and flows northwards on the western side of the Ridge.

The second watermass coming from the Nordic Seas flows over the Denmark Strait into the Irminger Sea. This Denmark-Strait-Overflow-Water (DSOW), forms together with the ISOW the Deep Western Boundary Current (DWBC). The DWBC, like the name suggests, flows southwards along the western boundary of the Atlantic Ocean. First around Greenland and around the Labrador Sea, before it continues along the Labrador and Newfoundland Coast, and further south (Bullister et al., 2013).

Section 2.2 already described deep convection in general and more specific in Labrador Sea. After the water has been convected, there are different pathways in which it can leave the interior of the Labrador Sea (Bower et al., 2011; Georgiou et al., 2020a). When leaving the Labrador Sea, the Labrador Sea Water (LSW) can be exported in different directions. Some can be exported in northeastern direction to the Irminger Sea. Another option is to be exported eastwards to the Mid-Atlantic Ridge, where it can either flow on the eastern or western side of it, to the south. The last option is to follow the DWBC further south, around Newfoundland and into the subtropics.

Figure 2.4 showed the different watermasses of the lower limb of the AMOC. If one thing has become clear, it is that it is a complex system of many different currents and water masses, connected through many different pathways.

2.4. Ocean Modelling

Numerical ocean circulation models and in a broader sense, Earth System Models, used for climate modelling, play an important role in oceanographic and climate research. These kind of models complement observational-based research (such as the OSNAP and RAPID/MOCHA arrays) since they allow for focussing on single processes and for research on larger space- and timescales.

Although the current generation of models is able to simulate a whole range of processes, still a lot of the physics that drive and influence certain processes, such as the AMOC, are not yet completely understood. This is reflected in the large range of projections made by different models, as can be seen in Figure 2.2.

When a model can approximate the mean strength of the AMOC quite well, it gives more confidence in the model to accurately capture the variability of the AMOC strength as well. It has been found that the mean AMOC strength of the ensemble of models participating in the Coupled Model Intercomparison Project (CMIP) represents the AMOC quite well (Weijer et al., 2020). The CMIP has designed several simulations that can be ran with the participating models. By running the same simulations can the results easily be compared. (Eyring et al., 2016) Since the variation in projections between models is quite large, but the mean is a good representation, the comparison of CMIP6 has become a important element in (international) assessments such as the reports of the Intergovernmental Panel on Climate Change (IPCC) (Eyring et al., 2016; Weijer et al., 2020).

The many coupled climate models, as seen in Figure 2.2, have a slightly different prediction on the AMOC strength. This is partly due to not yet completely understood physics that drive and influence the processes, but also due to how these physics are represented in the model.

Besides the physics and the processes itself, the numerical models itself also have their limitations. Global coupled climate models have a huge computational demand, especially when the entire climate needs to be simulated on a global (spatial) scale, on large timescales of several centuries and for different scenarios of atmospheric forcing. Modelling with a lower resolution grid is one of the options to decrease the computational demand. But in that case, more processes need to be parametrized as subgrid scale processes. An example of a process that needs to be parametrized in the current climate models, is the effect of unresolved mesoscale eddies that form the exchange between convection regions and downwelling regions.

Figure 2.2 shows that the projections of the AMOC strength by the different models follows a downward trend. Yet there are a lot of questions on how the processes associated with the AMOC are represented in the models, and how the AMOC will change under forcing by climate change. In this study, one of the models of CMIP6 will be looked at. It will be investigated how the different processes associated with the AMOC are represented in the Community Earth System Model (CESM) and how that affects the response to atmospheric forcing.

2.5. Problem definition and objective

In the above, it has been outlined what the Atlantic Meridional Overturning Circulation is and why it is important to have a good understanding of how it works and what it is driven by. The above also showed how we cannot only rely on observations for our understanding of the AMOC and that ocean models are a necessity, not only for the understanding of single processes, but also for the behaviour of the AMOC on longer timescales. This study focusses on the AMOC as simulated by the Community Earth System Model. By using both Eulerian and Lagrangian approaches, it will address the following main research question;

Does the decline in AMOC strength in response to increasing atmospheric greenhouse gas concentrations in a low resolution climate model like CESM constitute a reliable climate projection, considering our knowledge of AMOC dynamics?

The following subquestions will contribute to the formulation of the answer to the main question;

- Are the characteristics of the AMOC (overturning strength, spatial distributions of convection and downwelling) as simulated by the CESM model in agreement with the current knowledge based on literature and in particular on that deduced from higher-resolution models?
- How are the convection regions connected to the downwelling regions in the present-day control simulation of CESM?
- How do the characteristics of the AMOC in the sub-polar North Atlantic Ocean in the CESM model change in response to rising CO_2 concentrations in the atmosphere?

3

Specifications of the Community Earth System Model and OceanParcels

In this Chapter, the models and data used for this study are discussed. First, in Section 3.1 a general description of the Community Earth System Model (CESM) will be given, followed by a description of the output data from the model. The data will be used as input for the Lagrangian particle tracking software OceanParcels. Section 3.2 will introduce Lagrangian methods and this will be followed by a description of OceanParcels described in Section 3.3.

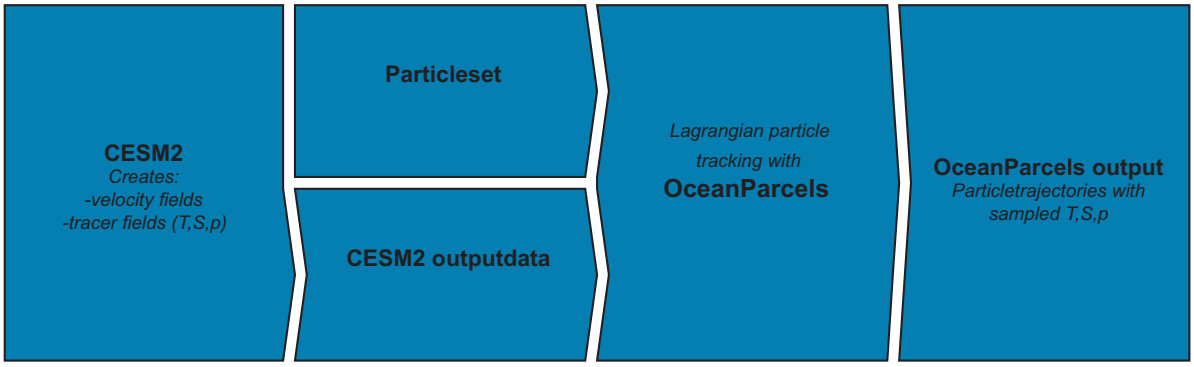

Figure 3.1: Flowchart of the data with CESM and OceanParcels.

3.1. The Community Earth System Model

The Community Earth System Model (CESM, version 2) is a fully coupled climate model developed by the National Center for Atmospheric Research (NCAR). The model simulates the different states of the global climate in the past, present and future. For each simulation a different configuration of components can be used that allows for the modelling of the different parts of the Earth System (Hurrell et al., 2013). A coupling between components means that a flux in one component, is a forcing for another component. For example, an increase in the CO_2 concentration in the atmosphere acts as a forcing for the AMOC strength in the ocean-component.

The most important component for this study is the ocean-component. The ocean model is the Parallel Ocean Program version 2 (POP2). The other components of the configuration are represented by the Community Atmosphere Model version 6 (CAM6) as the atmosphere model, the Los Alamos National Laboratory sea-ice model version 5 (CICE5) for sea-ice, the Community Land Model version 5 (CLM5) as the land model and the Community Ice Sheet Model version 2.1 (CISM2.1) as the land ice model (see Muntjewerf et al., 2020, and references therein for details). CISM models the Greenland Ice Sheet and has a so-called one-way coupling with POP (Lipscomb et al., 2019). So meltwater of the ice sheet affects the ocean, but the ocean does not affect the ice sheet. This coupling can influence the stratification of the ocean around Greenland and can thus have impact on the ocean circulation in the subpolar North Atlantic.

3.1.1. POP2 Specifications

As described above, is the ocean-component for the CESM2 model POP2. POP2 solves the hydrostatic primitive equations with a Boussinesq approximation (Danabasoglu et al., 2012). The Boussinesq approximation assumes that the density differences are small with respect to the density itself and that it does not affect the horizontal momentum equations. POP2 solves these equations on a fixed curvilinear, staggered B-grid. On a B-grid, the points where the velocities (u, v and w) and the tracers (T, S and ρ) are defined are not the same. Figure 3.2a shows an example of a gridcell. As can be seen in the figure are the horizontal velocities u and v defined in center of the vertical edges of the box. The vertical velocities w are defined in the middle of the top and bottom faces of the cell. Finally, the tracers T, S and ρ are defined in the center of the cell (Smith et al., 2010). Besides the B-staggering of the grid, also other ways to stagger a grid are possible in the form of A,C,D and E grids. These are not further discussed here. The way a grid is staggered has advantages and disadvantages on the different variables in the primitive equations. For coarse resolution grids, the B-grid provides the best results (Cushman-Roisin and Beckers, 2011).

Vertically, POP is a Z-level model. The model is discretized in 60 layers. The top 16 layers have a thickness of 10 meter. Between a depth of 160 meters and 3500 meters, the thickness of the cell increases from 10 meters up to 250 meters. From 3500 meters depth to the maximum depth of 5500 meters in the model, the cell thickness is 250 meters (Danabasoglu et al., 2020). The model does not have partial bottom cells, meaning the cells are completely filled with either land or ocean.

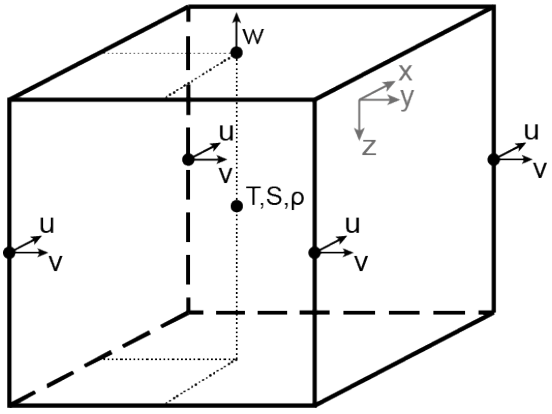

(a)

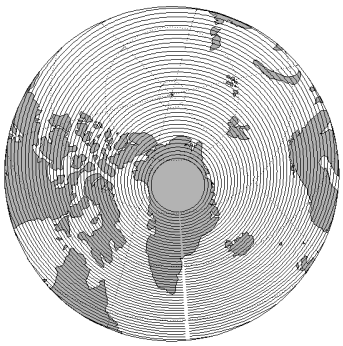

(b)

Figure 3.2: Illustrations of the curvilinear staggered B-grid. (a) shows an example of a grid cell, with the velocity and tracer points indicated. (b) shows the displacement of the grid northpole to the north of Greenland.

As CESM is a global climate model, POP also has to solve the ocean circulation in the Arctic Ocean. Increasing numerical instabilities near a pole force a model to keep a certain distance with the grid to the pole. When the poles of the grid are located on a landmass, like the South Pole on Antarctica, this is not a problem for an ocean model. As the North Pole is located in the Arctic Ocean, this is a problem. Therefore, the north pole of the grid in POP has been relocated to the north of Greenland, so that the north pole of the grid now is located in a land mass (Danabasoglu et al., 2020). This is illustrated in Figure 3.2b, where the circle of the grid around the new pole is visible.

Horizontally, the grid has a nominal resolution of 1°. The resolution of the CESM model is with 1° similar to most other models participating in CMIP6 (Weijer et al., 2020). Ideally, higher resolution climate models are used, as would increase the amount of processes that can be resolved. Higher resolution ocean-only models have shown that small scale processes such as mesoscale eddies, that cannot be resolved on a coarse 1° grid, play an important role in the AMOC and associated processes. It has been shown that in order to resolve mesoscale eddies in the model, one would need a grid with a resolution of at least 0.1° (Gent, 2013). Using a coarser grid is advantageous for the computational demand, but it implies also a loss of information, since smaller scale processes now belong to the subgrid scale. The loss of information on a coarser grid is illustrated with Figure 3.3. The figure shows the Sea Surface Temperature for two different POP simulations, one on a 1° grid and the other on a 0.1° grid. Small scale features, such as instabilities in the flow, are no longer resolved on the coarse grid. The use of a (too) coarse grid can alter solution of the model.

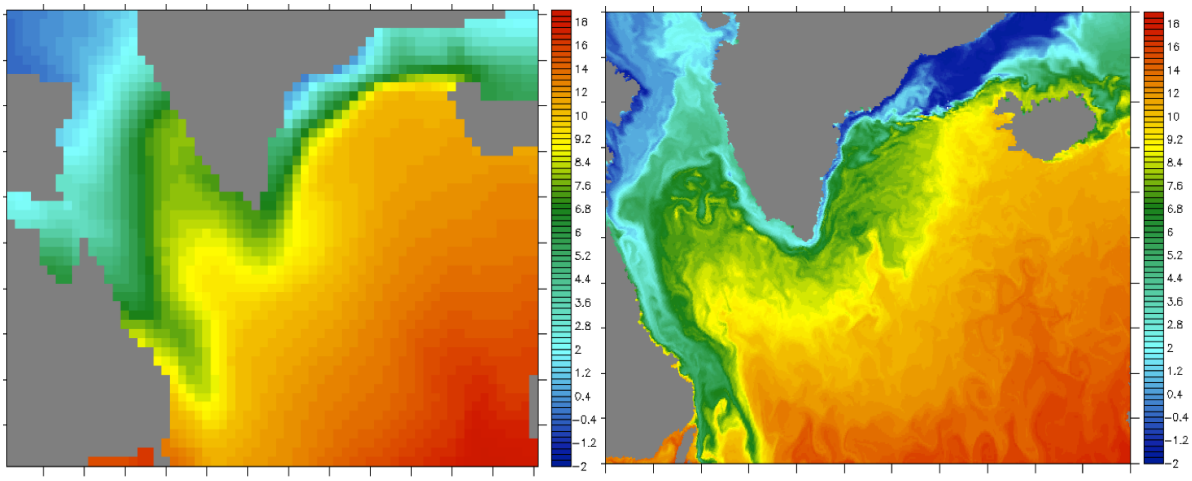

(a) (b)

Figure 3.3: Sea Surface Temperature in two POP simulations on (a) a 1° grid and (b) a 0.1° grid. (Courtesy of Prof. H.A. Dijkstra, Utrecht University)

3.1.2. Simulations and available data

The data used for this study is the output data from the POP ocean component of the CESM climate model. This data is the monthly means of the variables and this is obtained from two different simulations. The first simulation is a so called Pre-Industrial Control run (referred to as piControl), which after an initial spin-up time, has been run for 300 years. This control simulation is designed to be a baseline from which other simulations branch off (Eyring et al., 2016). The control run aims to establish a quasi-steady equilibrium of the climate under the conditions prior to the Industrial Revolution. For this, the year 1850 is taken as reference for the forcing. In this piControl simulation, the CO_2 concentration kept constant at a low value of 280 ppm. The second simulation starts after the piControl simulation. In this simulation (referred to as 1pctCO2) are the CO_2 concentrations in the atmosphere increased with 1% per year for a period of 140 years. After these 140 years, the CO_2 concentration in the atmosphere reaches a value of four times the initial concentration of 280 ppm and is kept constant for the rest of the simulation until the year 350. So from the years 140 to 350, given the long response time of the deep ocean and Greenland Ice Sheet, the model can further adjust to the new forcing from the atmosphere.

Figure 3.4 shows the AMOC strength, expressed in Sverdrups ($1\ Sv = 10^6\ m^3/s$), and the mean winter mixed layers depths for four marginal seas, for both simulations. The AMOC strength is marked with the black lines, the mixed layer depths with the colored lines. The figure clearly shows that the AMOC strength for the piControl (dashed lines) is constant in the long term, but shows some decadal variability. It also shows that when the atmospheric forcing starts increasing, the AMOC strenght rapidly drops for as long as the CO_2 concentrations are rising. When the forcing is kept constant again, the AMOC stabilizes at about 5 Sv.

For the analysis in this study, the data of two years is chosen. The first year of data is modelyear 300 from the piControl simulation (which is the last year of this simulation). The second year of data is modelyear 330 of the 1pctCO2 simulation. This is a significant amount of time after the CO_2 forcing is kept constant, so the system is in some sort of quasi-equilibrium.

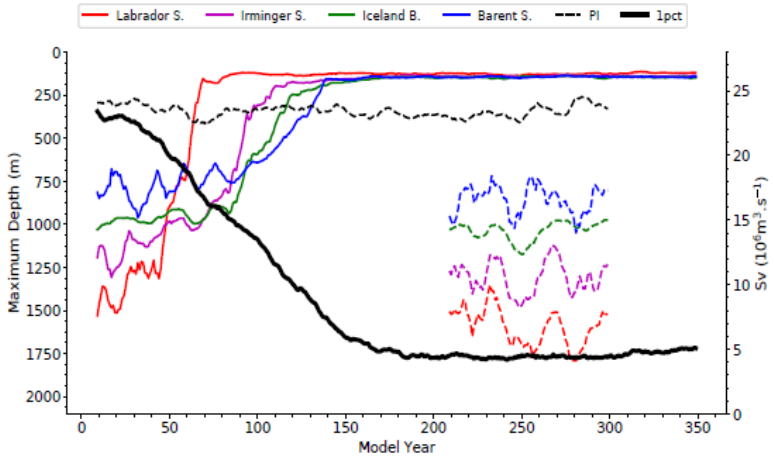

Figure 3.4: Strength of the North Atlantic Meridional Overturning Circulation Index (in Sv, black) and the local maximum mean January-Februari-March mixed layer depth within four regions: Labrador Sea (red), Irminger Sea (purple), Iceland Basin (green) and Barent Sea (blue). Dashed lines represent pre-industrial conditions (From Muntjewerf et al., 2020, their Figure 3.a)

3.2. Lagrangian methods

In a Lagrangian approach, the behaviour of a fluid parcel is being described in a framework in which the reference frame is moving with the fluid parcel. In contrast to a Eulerian approach, in which the reference frame is fixed. Part of the output of many ocean models, including POP2 used in this research, is a 3D velocity field in a fixed grid (van Sebille et al., 2018). A Eulerian approach is useful to get information on for example the variability of the AMOC or the formation of deep water. The Lagrangian approach gives insight in the three dimensional structure of the flow and the pathways of water masses (Bower et al., 2019).

The Lagrangian analysis uses virtual particles, which can represent water masses or other properties, such as temperature or salinity. The particles use Eulerian information of the fluid, for example from a stored velocity field, and are being advanced by interpolating through the velocity field to get a trajectory (Delandmeter and Van Sebille, 2019). This is illustrated in Figure 3.5, where the first 5 timesteps are plotted from a parcel in the piControl simulation. Once the parcel is advected, one can store the information from tracers, such as temperature or salinity, at that location and time.

For the use of Lagrangian analyis there are two methods. The first method, online computing, calculates the position of the particles at each timestep the model is updated. The second method, offline computing, is the method that will be used in this research. While performing a model simulation, the velocityfield is stored at certain time intervals. Once the velocity field of the model is known in time (the available years of data), this allows for two ways of calculating the pathways of virtual particles: either forward computing of the trajectories, in which the particles are followed forward in time, or backward computing of the trajectories (van Sebille et al., 2018). Backward computing is useful to find where a water mass originates. Forward computing can be used to see where a water mass goes.

A problem that may arise is that many processes in the ocean take longer than the period the data set covers. A commonly applied method to overcome this problem is to loop the velocity field while computing the particle trajectories. When this is applied, the differences between the beginning and end of the data, the point where the loop is closed, need to be small. Large differences can be cause for large errors or unphysical behaviour (van Sebille et al., 2018). Large differences may arise if the model is in a transient state, for example like the first 140 years of the 1pctCO2 simulation.

For the Lagrangian analysis in this study, the data of the selected years is looped. First, this is because interpretation of the results becomes very difficult when the model is in a transient state, which is the case for the 1pctCO2 simulation because of the long response time of the deep ocean and the Greenland Ice Sheet to forcing. Second, looping the data reduces the amount of data that is input for OceanParcels. This applies to both the piControl and the 1pctCO2 simulations.

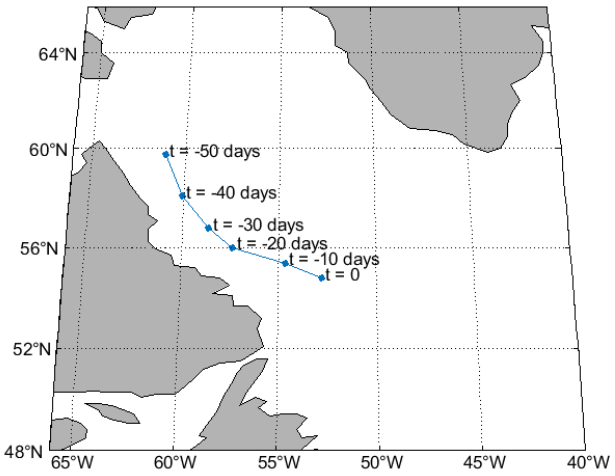

Figure 3.5: Example of backward computing of a parcel trajectory, showing the first five timesteps of a parcel in the piControl simulation

3.3. OceanParcels and its use in a coarse model

The software that will be used for the Lagrangian analysis of the AMOC in the POP output data is OceanParcels. Parcels ("Probably A Really Computationally Efficient Lagrangian Simulator" Delandmeter and Van Sebille, 2019) is Python-based software that can be used for the tracking of watermasses by creating virtual particles that can be 'released' in the POP output data.

The output data from POP is provided to Parcels as Fields. The Fields contain the grid and the points at which the information is provided, such as the velocity data (Delandmeter and Van Sebille, 2019). The data provided to Parcels for the fieldset contains the three velocity components u, v and w, the data of different tracers (temperature, salinity and density) and the variable of the mixed layer depth. Parcels uses a fourth order Runge-Kutta scheme to advect the particles through the fieldset. However, particles are almost never exactly on a gridpoint and interpolation of the fieldset is necessary to find the local values attributed to the particle. Parcels takes into account the type of grid-staggering by the model, the B-grid in the case of POP2. Parcels uses a linear interpolation method to interpolate the velocities. For tracers, the value is constant in the cell (Delandmeter and Van Sebille, 2019).

The behaviour of particles can also be customized. In Parcels, Kernels are being used to change the behaviour of the particles. Some simple kernels have been used to for example remove particles that gave an "Out of Bounds Error" from the particleset or to make the fieldset periodic in zonal direction.

Parcels reads cells with a zero value as land cells. The interpolation method causes the velocities near land boundaries to rapidly decrease. This causes a lot particles to get 'stuck' in the steep bathymetry of the Labrador Sea during testruns. This is a consequence of the coarse grid and the interpolation method. In order to prevent particles being stuck for the remaining of the simulation, the advection-kernel has been expanded with the snippet below to address the issue with the stuck particles.

```
if math.fabs(prev_lon-particle.lon)<=1e-4 and math.fabs(prev_lat-particle.lat)<=1e-4:
    r = 1/3.
    delta_x = random.uniform(-1.,1.)*math.sqrt(2*math.fabs(particle.dt)*25./r)/(1852*60.)
    delta_y = random.uniform(-1.,1.)*math.sqrt(2*math.fabs(particle.dt)*25./r)/(1852*60.)
    particle.lon += delta_x
    particle.lat += delta_y
```

The code gives a random horizontal displacement to the particle if the horizontal displacement during a timestep comes below the chosen threshold. The threshold is met when both the meridional and zonal displacement are less than 10^{-4} degree or equivalently 11 meter during a timestep of 1 hour. With an average velocity of about

10 cm/s in the boundary current, the 'normal' displacement during a timestep would amount to 36 meter, a factor 3.6 times larger.

If the threshold for the random displacement is met, the particles are displaced by approximately 700 meter (or 0.006 degree) times a random factor in both meridional and zonal direction. The result is a displacement in a random direction with a maximum of 990 meter. This maximum is only reached when both directions have a maximum random factor.

This random displacement is not able to prevent all particles hitting the land. The random displacement is unphysical behaviour what is added to the trajectories. This behaviour is acceptable to get insight in the trajectories they travel and the tracers they sample. For which a displacement directed at the center of the circulation would be less ideal.

It should be noted that the Lagrangian methods as described above, open up a whole range of opportunities for statistical and probabilistic analyses. It would be possible to calculate volume transports based on the particle trajectories (e.g. Döös, 1995) or to bin the locations of particles for different probabilistic analyses (e.g. van Sebille et al., 2018). However, the relatively large kick needed in this coarse model to keep the particles going on their trajectories means that such analyses would be unreliable. Furthermore, the high viscosity due to the coarse grid in the CESM model, makes that there are apparently no different pathways between an interior and a boundarycurrent in for example the Labrador Sea. Chapter 5 will elaborate on this. The results in this study will therefore be mostly a qualitative analysis, instead of a quantitative analysis as well.

3.4. Summary

For this study, the characteristics of the AMOC in the CESM model will be analysed. The CESM model is a fully coupled climate model, with which the past, present and future of the climate system can be modelled. The main component of the model for this study is POP, the ocean component. In this study, two simulations made with CESM are used. The piControl simulation is a reference simulation, which can be used to compare the AMOC characteristics with for example literature and other models. For 1pctCO2 simulation, the concentration of CO_2 in the atmosphere is increased with 1% per year for the duration of 140 years. After 140 years, the concentration is kept constant for the rest of the simulation. The data of year 330 has been used.

The output data from CESM is input for Parcels. With Parcels, a Lagrangian analysis of the model can be done by tracking virtual particles through the velocity fields. At each timestep, the particles can sample the values of tracers, such as temperature, salinity and density. Besides the velocity and tracer fields from the CESM model, Parcels also needs as input a description of where and at what time the particles are seeded into the ocean.

The next chapter will elaborate on the Eulerian analysis of the model as well as the considerations taken for the construction of the particleset.

4

Research approach

This chapter gives a description of the steps taken in the analysis of the AMOC in the CESM model. The chapter is split into two sections. The first section will identify what information can be gained from a Eulerian perspective of the CESM model output data. The second section will do the same, but from Lagrangian perspective. This section will address the input data needed for Parcels and the considerations made in the use of the software.

4.1. Eulerian approach

First, the AMOC will be characterized from a Eulerian perspective. Section 2.2 explained the convection process. It outlined that water masses are transformed when they are located in the mixed layer. So the first step is to look how the mixed layers are distributed over the area and in time in the CESM model. The second key characteristic of the AMOC is the vertical transport of the convected waters. So it is necessary to look into the vertical velocity field from the CESM model. Where can the largest velocities be found and how does that relate to the locations where deep mixed layers are found?

From Muntjewerf et al. (2020), the mean meridional streamfunction of the northern Atlantic Ocean is known, see Figure 4.1. The streamfunction is the vertical integral of the zonally integrated meridional velocity. The streamfunction is a measure of the AMOC strength, as one can see how much water flows north or south. The maximum of the streamfunction indicates at which depth the maximum of the overturning occurs, where most of the vertical transport happens (Sayol et al., 2019). Figure 4.1 shows the 20 year averaged streamfunction in different periods of the simulation. The upper frame shows that the maximum of the overturning (streamfunction) in the piControl simulation can be found at a depth of approximately 1000 meter. This is thus also the depth at which most of the vertical transport occurs, and therefore, this will be the initial depth to look at the spatial variations of the vertical velocity field of the model.

First of all this will be done for the piControl run. After that, the same will be done for the situation after the CO_2 forcing.

4.2. Lagrangian approach

The Eulerian approach gives insight in where convection occurs in the CESM model and where the overturning occurs. This Eulerian approach does not show how the two different components of the AMOC are connected. A Lagrangian approach can give this insight. Section 3.3 described the data that is input for Parcels. In this section, the data that forms the particle set is discussed.

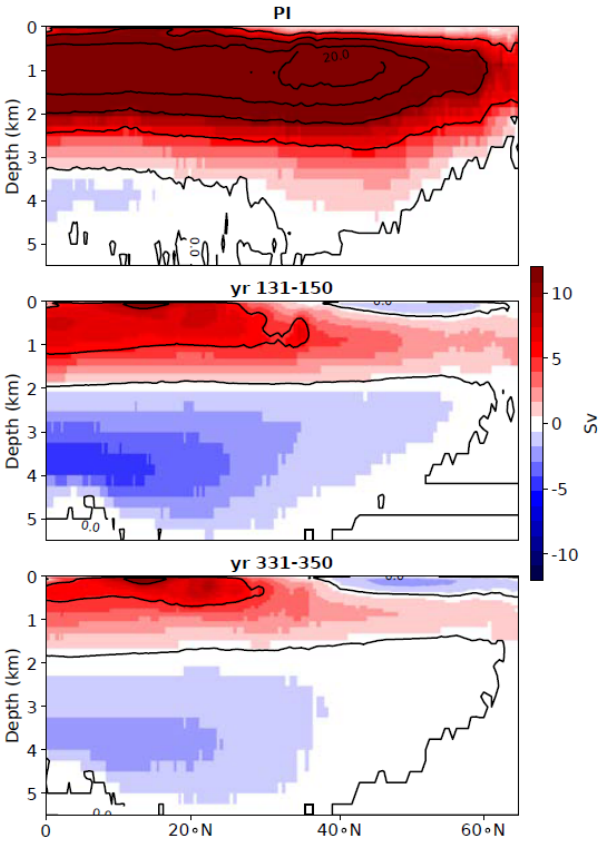

Figure 4.1: Mean Meridional Streamfunction of the northern Atlantic Ocean, averaged over 20-year periods in different periods of the simulation. The streamfunction of the piControl simulation can be found in the upper panel, the lower two panels belong to the 1pctCO2 simulation (From Muntjewerf et al., 2020, their Figure 3.b)

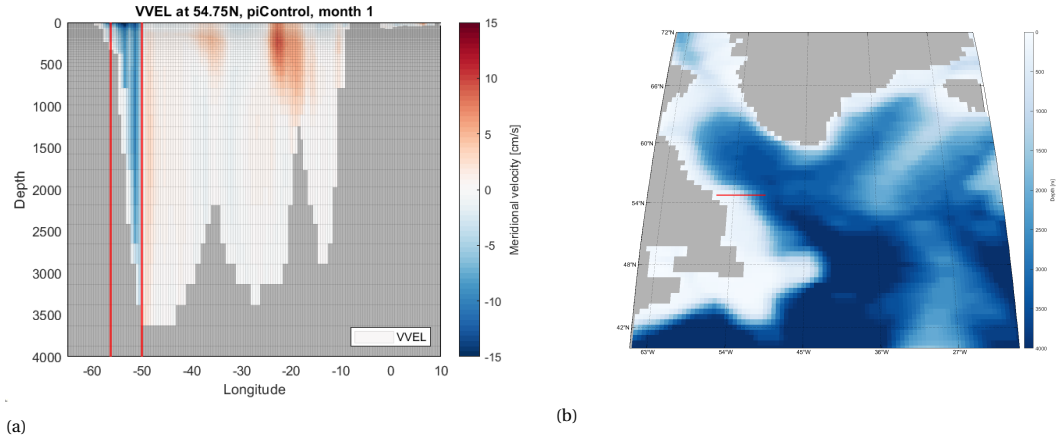

Figure 4.2: Cross-section at 54.75°N of the meridional velocity in the first month of (a) the piControl simulation and (b) a map of the starting location. The particles are being released between the two red lines.

4.2.1. Location

Section 3.3 showed that it is possible to trace the particles either forward or backwards in time. To find the pathways of the convected waters in the CESM model, it thus possible to release the particles either in 'upstream', the upper limb of the AMOC, or 'downstream', in the lower limb of the AMOC.

From Section 2.3 it became clear that AMOC is a complex structure of different water masses. In the upper limb, the water masses come from different directions and flow to the different convection areas in the marginal seas. This makes it difficult to use a single release location for the particles.

In the lower limb, the general direction of the flow is in one direction. The convected waters coming from the different marginal seas all end up in the DWBC, from where they flow further south. The DWBC flows around the edges of first the Irminger Sea and then around the Labrador Sea. This makes the DWBC on the western side of the Labrador Sea a suitable location to release the particles from.

In order to determine the exact location for the release of the particles, the DWBC in the CESM model needs to be found. Figure 4.2 shows a cross-section at $54.75^\circ N$ of the meridional velocity in the piControl simulation. In the cross-section of the piControl simulation the DWBC is clearly visible with blue colors on the left side of the figure.

The particles are released from a section at $54.75^\circ N$, between 56.25° W and 50° W. This is marked with the red lines in the cross-section and map of Figure 4.2.

4.2.2. Time

The deep convection process has a strong seasonal character. During the winter months the cooling by the atmosphere is strong enough to allow for deep convection to happen. In the rest of the year, the ocean restratifies, which blocks the convection process.

The seasonal character of the mixed layers and ocean circulations underlines why it is important to release particles at different times. If all particles are released at the same time, it can happen that only the faster (c.q. slower) particles experience convection.

The outputdata from the CESM model is monthly averaged. Therefore, an array of particles will be released from the starting location every month.
Section 3.2 explained why the data of a single year is looped for the duration of the simulation. The looping of a single year of data implies that particles released in the first month of the second year will have the exact same trajectories as the particles released in the first month of the first year and hence, particles only need to be released during the first year of the simulation, at intervals of one month.

The goal of the Lagrangian particle tracking is to see where the convection and overturning occur. Georgiou et al. (2020a) already showed that the convection pathways in the Labrador Sea alone are in the order of several years. This can differ for the CESM model, but it is probably in the same order of magnitude. TO not only trace the particles through the Labrador Sea, but also have them enter the Irminger Sea in the simulation, is the duration of the simulation set to 15 years.

4.2.3. Number of particles

A single particle can give insight in the transformation of tracers such as temperature, salinity and density along the particle trajectory. But a single track is not enough to give insight in the movement of a watermass. To track the entire watermass, a large set of particles is needed.

The particleset used for the simulations with Parcels consists of 125 particles horizontally on a line between $56.25^\circ W$ and $50^\circ W$. With 125 particles, the horizontal distance between two particles is 0.05°, or at this latitude, approximately 3200 meter.

Considering that the grid of POP has a resolution of 1°, a horizontal distance of 0.05° is sufficient to track the water masses. The coarse grid resolution makes that the differences in the velocity field after interpolation are small and that an even smaller horizontal distance between the particles is not necessary.

Figure 4.3 shows the distribution of the particles at the release location. Vertically, there are 60 rows of particles, equally spread out between a depth of 50 meters and 3000 meters. Consequently, the vertical distance between two lines of particles is 50 meter. With 125 particles horizontally on a line and 60 particles above each other, the total array of particles contains 7500 particles. The particles will only be released from ocean grid boxes.

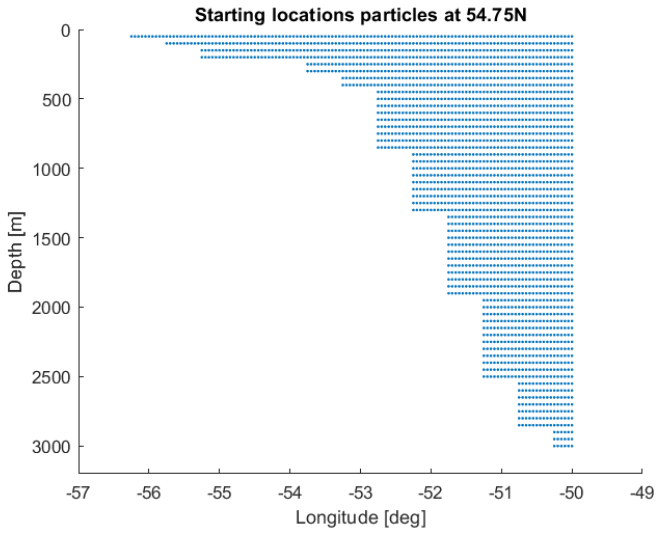

Figure 4.3: An overview of the distribution of the particleset at the starting location of the simulation.

Particles initially located in a grid box that contains land are removed from the particleset. After removal of these particles, does the resulting array of particles have a size of 2530 particles. A single release contains 2530 particles. When released during an single year in sets of 12, the total number of particles being released is 30360 particles.

4.2.4. Summary of the total particleset

In summary, the particles in Parcels are released from a line at 54.75° N, between 56.25° W and 50° W. The particles cover the entire cross-section over that line, the highest particles start at a depth of 50 meter and the deepest particles can be found at a depth of 3000 meter. The particles have a horizontal distance between them of 0.05° and a vertical distance of 50 meter. The set is an array with horizontally 125 particles and 60 particles vertically. After removal of the particles in land grid cells, is the size of the remaining set 2530 particles. When released on a monthly basis during the first year, the total particleset is 30360 particles.

In the Parcels script, the particles are being advected with a timestep of $\Delta t = 1$ hour for the duration of 15 years. Outputdata containing the location of the particles and the sampled values of temperature, salinity and density at those locations, is written to an outputfile at an interval of 10 days.

5

Analysing the piControl simulation

Following the structure and approach as outlined in Chapter 4, this chapter will present the results of that approach for the piControl simulation. It starts with a Eulerian analysis of the mixed layers and vertical velocities. This gives a background for the Lagrangian analysis of the piControl simulation, in which particle trajectories are analysed to find the connection between convection and downwelling.

5.1. Eulerian analysis

5.1.1. Mixed Layers in the northern Atlantic Ocean

Section 2.2 showed that when convection occurs, deep mixed layers will be present in the ocean. These mixed layers can be used to locate where convection occurs. The deep mixed layers are present in the first four months of the year, spread out over the Iceland- and Irminger Basins and the Labrador Sea. Figure 5.1 shows the area and depth of the mixed layers during March. In this month the deep mixed layers cover the largest area and they reach a maximum in the Labrador Sea. This deepest point can be found at a depth of 1661 meter.

In the figure it can be seen that the mixed layers are present in the entire interior of the Labrador Sea, but it also covers some part of the boundary current on the eastern side, near the coast of Greenland.

During the other months, the ocean restratifies and the deep mixed layers disappear. What is left are mixed layers induced by the atmosphere, mostly in the order of about 100 meter.

The locations in which the mixed layers are found are similar when compared to other ocean models, for example as found in Katsman et al. (2018). The location of the deepest mixed layers is similar to their ORKA1 simulation, in which the mixed layers are close to the continental slope on the western side of Greenland. For their higher resolution ORCA025 simulation, the location is slightly different. The higher resolution model shows the deep mixed layers closer to observations, for example from Pickart et al. (2002).

Where the location is comparable, there is a large difference in the depth to which the mixed layers extend. Where in the simulations of Katsman et al. (2018), mixed layers can be found at depths well over 2000 meter, with 2255 m for ORCA025 and 2882 m for ORCA1, are the mixed layers in this piControl simulation in the CESM model with a maximum of 1661 meter quite shallow. The mixed layer depth in models is, as it is also the case for observations, a consequence of the ocean properties and the applied forcing. Observations (Gelderloos et al., 2013, and references therein) show a wide range of mixed layer depths between approximately 1000 - 2300 meter. The mixed layer depth found in the CESM model is in the range that LSW can be produced by the model.

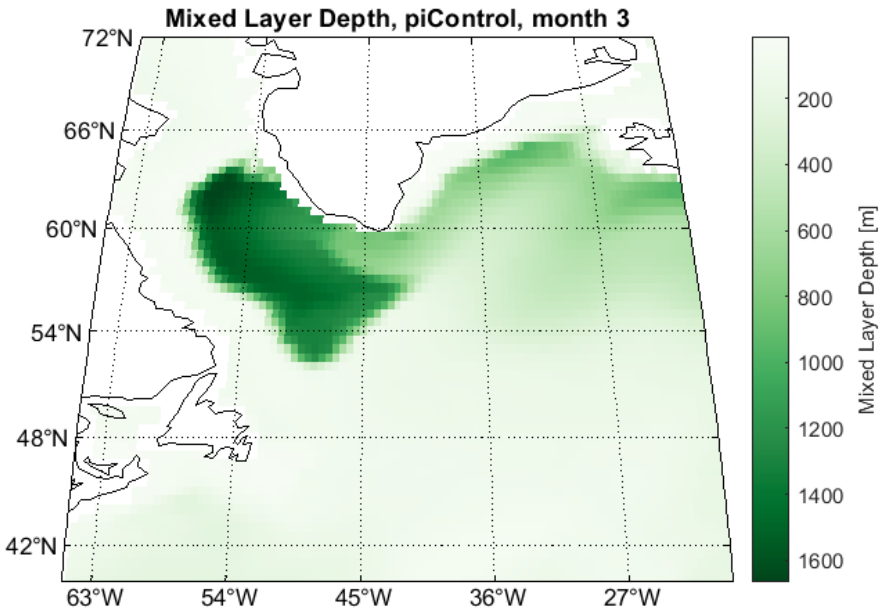

Figure 5.1: Mixed layer depth in the northern Atlantic Ocean in March (month 3 of the dataset)

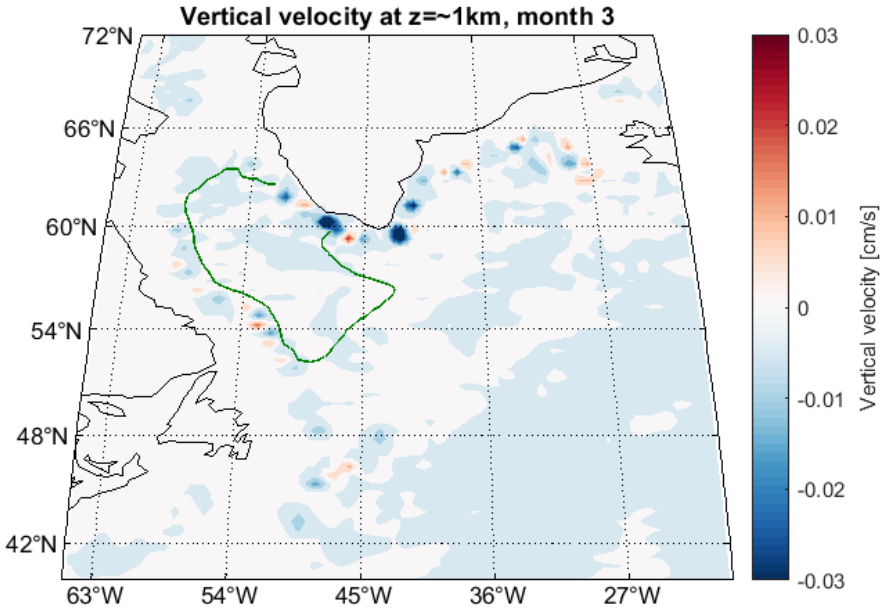

Figure 5.2: Vertical velocities in March (month 3 of the dataset), the 1000m mixed layer depth contour is indicated in green

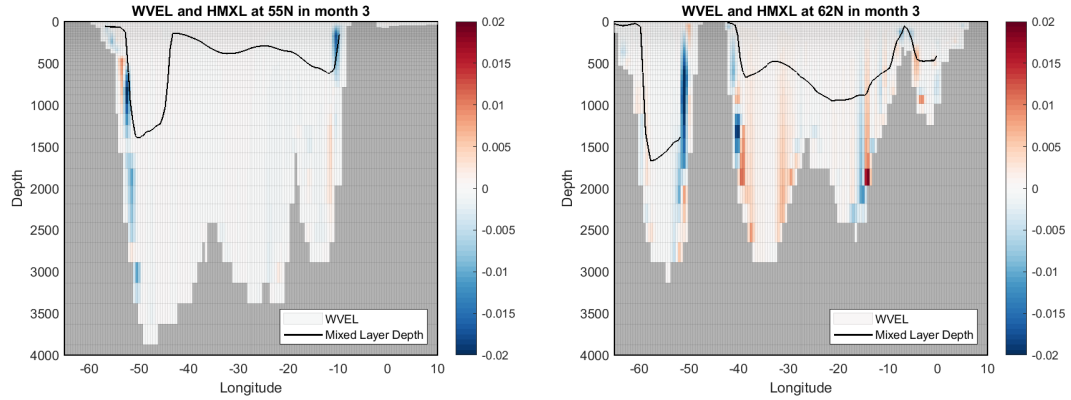

Figure 5.3: Cross-sections of the vertical velocities at (a) 54.75°N and (b) 61.75°N, with the mixed layer depth indicated in black

5.1.2. Overturning in depthspace, vertical velocities

Figure 4.1 showed the mean meridional streamfunction. From the top panel in this figure, it can be deduced that the maximum of the streamfunction can be found at a depth of approximately 1000 meters. This is the depth at which the largest vertical transport occurs.

Figure 5.2 shows a map of the vertical velocities at a depth of 984 meter. Downward velocities are marked with blue. Also indicated in the same figure is the 1000 meter contour of the mixed layer depth, during the third month.

The figure shows that vertical (downward) velocities can be found in the entire Atlantic. It also shows that these velocities are in general in the order of 0.01 cm/s and smaller. Although, integrated over the entire width, of the ocean, does this still imply a large vertical transport, to be exact, this adds up to the 25 Sv that is displayed in Figure 3.4

In the interior of the Labrador Sea, the velocities are similar to the velocities found in the open ocean. Larger velocities, both up- and downward, can be found over the steep continental slope. The cross-sections of Figure 5.3 support this view, where the larger vertical velocities are found over the steep continental slopes and minimal velocities in the interior of the Labrador Sea. Also indicated in this figure are the mixed layer depths. These cross-sections show that the largest vertical transport occurs in a different place than where the mixed layers are located.

Spall and Pickart (2001) derived an equation that quantifies the amount of sinking near a boundary around a convective basin. It showed that the larger velocities over the continental slope are induced by horizontal density gradients along the boundary. Katsman et al. (2018) adapted their equation so it uses the depth at which the maximum vertical transport occurs (see Equation 5.1, equation (1) from Katsman et al. (2018));

$$W_b = \frac{g\Delta\rho_B z_{sink}^2}{2\rho_0 f}, \tag{5.1}$$

in which W_b is the overturning near the boundary, g is the gravitational acceleration, $\Delta\rho_B$ is the horizontal density gradient and ρ_0 a reference density, z_{sink} is the depth of the maximum vertical transport and f is the Coriolis parameter. Figure 5.4 shows the variation of the vertical velocities taken at $50,25°W$, $61,75°N$. Equation 5.1 can be used to explain the variability in the vertical velocity at this point. The density gradients are not only caused by the presence of mixed layers near this boundary. Other factors create density gradients as well, for example atmospheric cooling and mixing by mesoscale eddies (Katsman et al., 2018). The first two factors, the presence of the mixed layers and the atmospheric cooling increase the vertical transport in the first half of the year, while the last factor, the mesoscale eddies, are, if present, a factor that lessens the difference between the first and second half of the year, as they create density differences around the year.

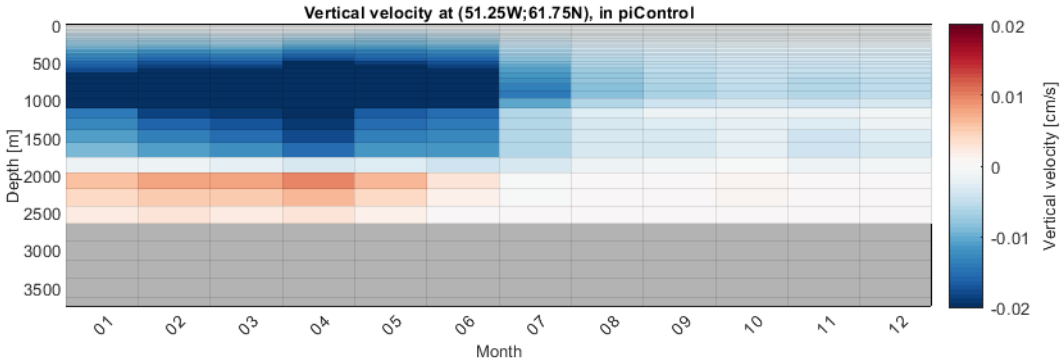

Figure 5.4: Variability of the vertical velocity over time at (51.25W, 61.75N)

5.2. Lagrangian analysis

The Eulerian analysis showed that both components of the AMOC, convection and downwelling, are present in the model, at the location where it is expected to be found, the convection in the interior and the downwelling over the steep continental slopes. In order to find the pathways of the water masses and how the AMOC parts are connected, particles are released using Parcels.

5.2.1. Particle pathways in the subpolar gyre

Based on Section 2.3, the picture is sketched of an AMOC consisting of a complex system of different currents coming from and going to many different directions. A reasonable expectation is that this would be reflected in the particle trajectories as found by Parcels. As stated in Section 4.2.3, a total of 30360 particles have been released, divided over the twelve months of the first year of the simulation and these particles have been traced backwards in time for 15 years. Figure 5.5 shows a selection of 491 particle trajectories. The selection of particles in the figure is based on the criterium that the particles have maximum of 20 random movements caused by the kernel that was described in Section 3.3. This selected only the particles that have spent minimal time in or near the land boundary, as the kernel is only applied when the particles displacement is smaller than the threshold.

Figure 5.5 shows that most of the selected particles flow as a single viscous flow through the subpolar gyre. While most of the particles flow are closing the loop of circulation in the subpolar gyre, only a very limited number has an origin elsewhere than the subpolar gyre. A few particles enter the subpolar gyre through either the Hudson- or Davis Strait. Since the waterdepth in these locations is shallow, are this particles that are located near the surface, and thus not relevant for tracing convection and downwelling in the model. Furthermore, it is expected that some (surface) particles would find their origin in the upper limb of the AMOC, and thus most probably would enter the subpolar gyre in this simulation through the Gulf Stream, but none of the selected particles does have this pathway.

This view is supported by a simulation in which the particles are traced forward in time from the starting location. The 2530 particles of this simulation are released in the first month of the simulation. No selection has been made based on for example the amount of random movement that has been applied. In the backwards simulation, most particles got stuck in the steep bathymetry of the Labrador Sea. This is not the case in this forward simulation, where the particles first enter the open ocean. Figure 5.6 shows the trajectories of this simulation. This figure shows that most of the particles keep circulating in the subpolar gyre, but opposed to Figure 5.5, it is possible to distinguish a clear export pathway to the subtropics. The particles and their trajectories using this pathway will be referred to as ExportSouth particles. These particle trajectories are marked in orange in the figure.

Remarkable is that this seems to be the only export pathway of water coming from the Labrador Sea to the subtropics. Opposed to the findings of Section 2.3, in which the pathways to the south were either to follow the DWBC, or to follow the Mid-Atlantic Ridge. A possible explanation for this is that the flow to the south is being blocked by the NAC in the model. Only on the eastern side of the Atlantic, where the flow of the NAC weakens, it is possible for the particles to cross the NAC and flow southwards.

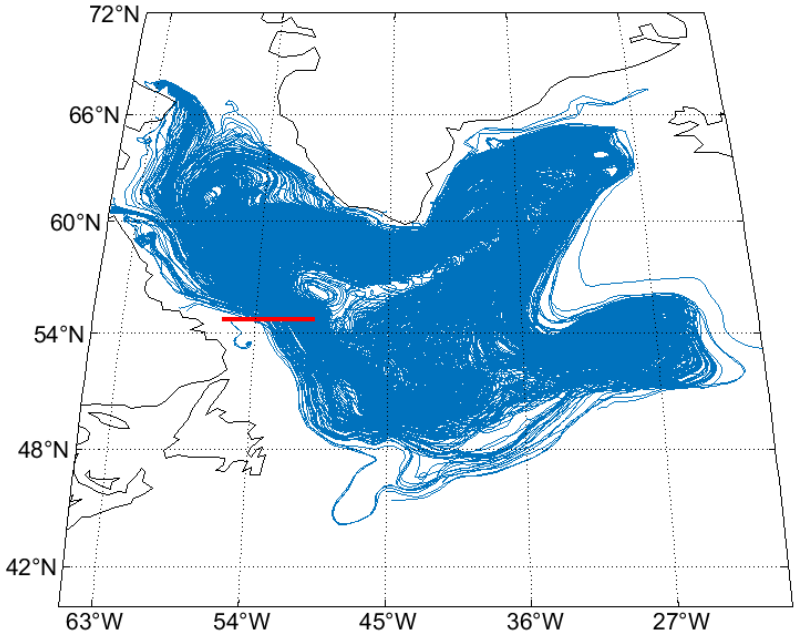

Figure 5.5: Trajectories for a selection of 491 particles. The particles are traced backwards in time for a duration of 15 years. The starting location is marked in red.

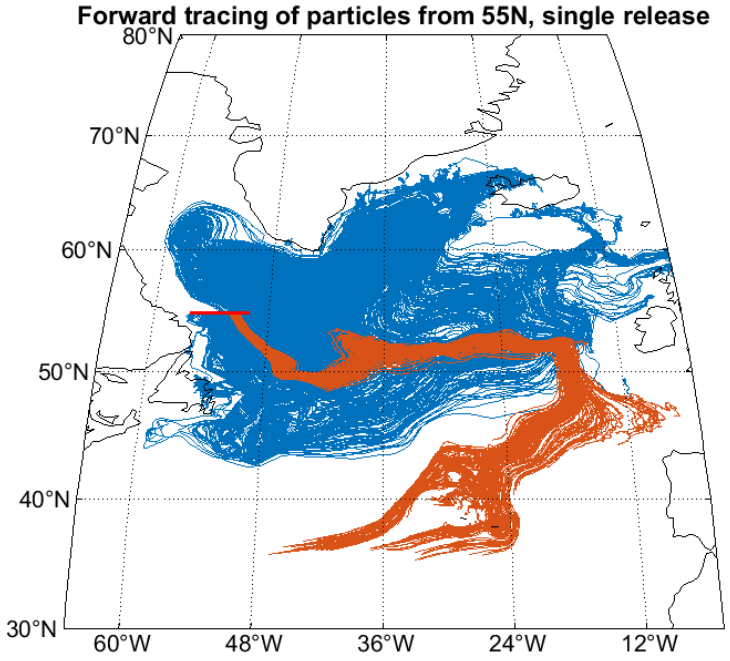

Figure 5.6: Trajectories of 2530 particles. The particles are traced forwards in time for a duration of 10 years. The starting location is marked in red. The trajectories of ExportSouth are marked in orange.

In Section 2.2 it was described how Georgiou et al. (2020a) showed that it is possible to distinguish different pathways of the particles. These pathways were based on when and where they would leave the boundary current (or not) and enter the interior of the Labrador Sea, where the convection occurs. The trajectories shown in Figure 5.5 clearly show that such a classification would not be useful on the particles in this simulation. In this simulation there are no different pathways between an interior of the sea with convection and a boundary current with downwelling. Still, the Eulerian analysis showed that convection can be found in the interior of the sea and downwelling in a narrow region over the steep continental slopes. The implication is that particles can go through convection, but do not have downwelling. The main pathway the particles follow, crosses the Labrador Sea through the interior, before it flows closely around Cape Farewell after which it turns northwards. So particles experience convection when they cross the interior at the time the mixed layers are present. It is similar for the downwelling, the particles can experience downwelling, if their trajectory is close enough to the steep continental slope.

5.2.2. Example of a particle experiencing overturning in density space

Both this section and the next section will look closely at examples of trajectories and the overturning of the particles in both depth- and density space. The simulation traced the particles backwards in time, starting at $54,75^\circ$ N. For the clarity of the description, the description will follow the particles forward in time, starting the description in the upper limb of the AMOC, and then follow the particles in downstream direction until they arrive at the starting location.

Figure 5.7 shows an example trajectory and the properties along the trajectory of a particle, that has a change in density, but does not experience a change in depth. The total duration of the simulation was 15 years, but only the first 600 days of the particle trajectory are shown. Because as can be seen in the two maps (a and b) of the figure, the entire track of the particle is shown as the gray line, which ends up being stuck soon after 600 days of the simulation. This particle was part of the subset that was released during the fourth month, which is why Figure 5.7c, ends on day -100 of the simulation.

Figure 5.7a shows the trajectory of the particle from the east side of Greenland to the starting location at $54,75^\circ$ N. The colors of the dots display the difference between the depth at the current location and the particle depth when it reaches $54,75^\circ$ N. It can be seen that the vertical displacement during the entire simulation is minimal (less than two meters). For Figure 5.7b is this different, which shows, for the same particle, the difference between the particle density at the current location and the particle density when it reaches $54,75^\circ$ N.

The panels of Figure 5.7c show the change of the particles temperature, salinity, density and depth over time. As can be seen in the top panel of this figure, there are small changes in the particles temperature when its located on the east side of Greenland (this corresponds to the left side of the panel). These changes cause also small density changes. The strongest change in density occurs when the particle is located in the mixed layer (see bottom panel of the figure), this occurs in the region around Cape Farewell. As can be seen from the top panel, this change in density is mostly a consequence of a strong cooling of the particle.

In the last part of the trajectory, between leaving the mixed layer and the starting location at $54,75^\circ$ N, the particle crosses the interior of the Labrador Sea. In this part of the trajectory, the changes to the particle properties temperature, salinity, density and depth are nihil.

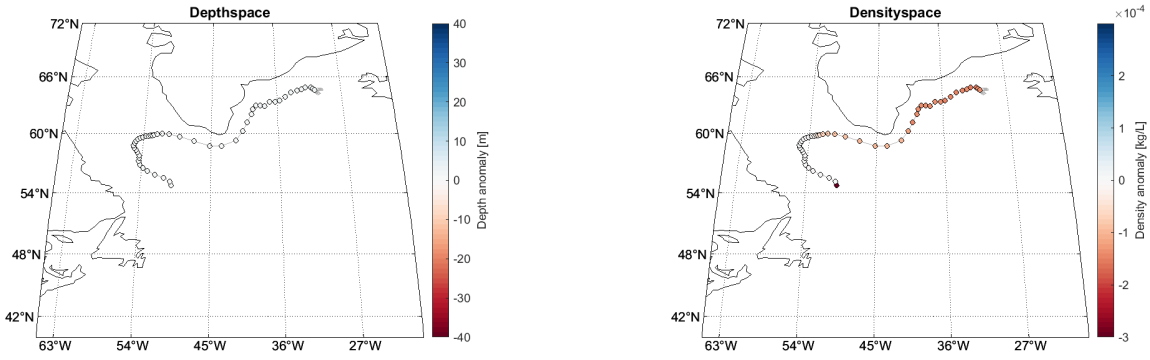

(a) (b)

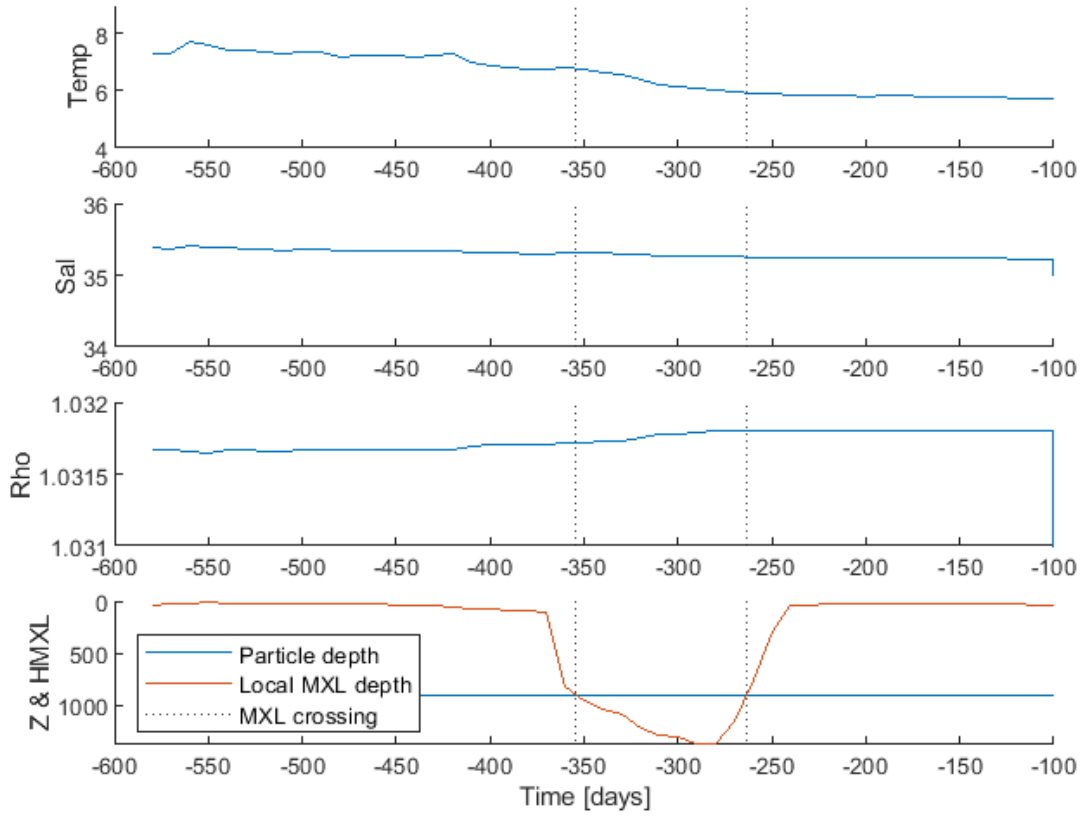

(c)

Figure 5.7: Example trajectory illustrating overturning in density space. The depth anomaly compared to the particle depth at $54,75°$ N is plotted in (a), in (b) the density anomaly compared to the particle density at $54,75°$ N is plotted. (c) showsthe particles temperature, salinity and density over time as well as the depth (all in blue). The bottom panel of (c) also shows the local mixed layer depth marked in orange.

5.2.3. Example of a particle experiencing overturning in depth space

Besides an overturning in density space, as shown above, can a particle also experience an overturning in depth space. This occurs when the trajectory of the particle is close enough to the continental slopes, where the strong vertical velocities are found. Figure 5.8 shows the difference in depth of a particle versus the difference in density of the particle. This difference is calculated between when the particle crosses $40°W$ and when the simulation started at $54.75°N$. The colors indicate the depth of the particle at $54.75°N$. The figure shows that surface particles are constantly affected by the atmosphere and therefore display a large range of density differences. Deeper particles all experience a density change when the trajectory crosses the mixed layers in the interior of the Labrador Sea, but only in a few cases is the trajectory also close enough to the continental slopes and is there a change in depth.

Figure 5.9 shows a example of a particle that shows also a large change in depth, besides the change in density. The particle trajectory in this example is much closer to the continental slopes for a longer duration than it was the case for the example of Figure 5.7.

The example trajectories in this section and the previous section, clearly show that the AMOC is not only determined by the AMOC strength. The particles move as a viscous flow around the subpolar gyre. The particles experience convection while they move through the deep mixed layers in the interior of the Labrador Sea, but only a small part of the particles has an individual trajectory that is close enough along the continental slopes for the particle to also experience downwelling.

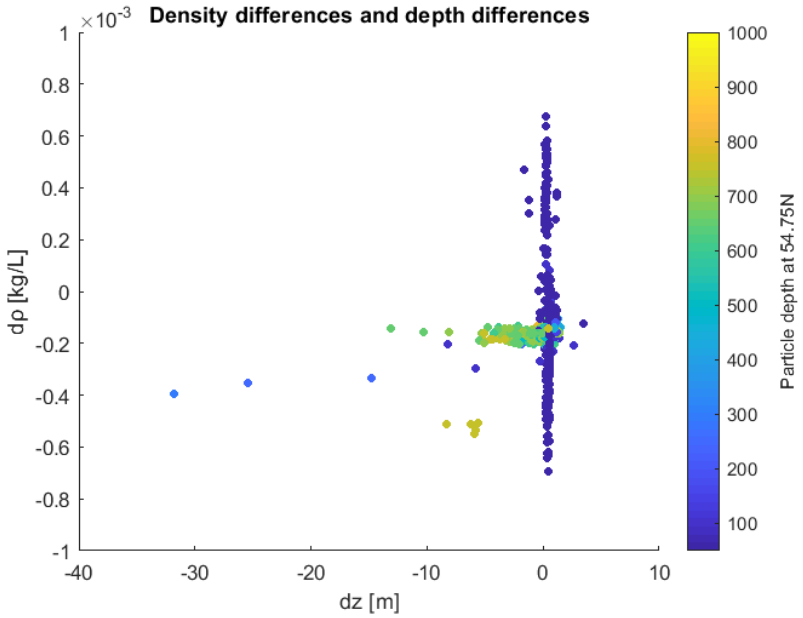

Figure 5.8: The change in depth versus the change in density between $40°W$ and $54.75°N$. The colors mark the particle depth at $54.75°N$.

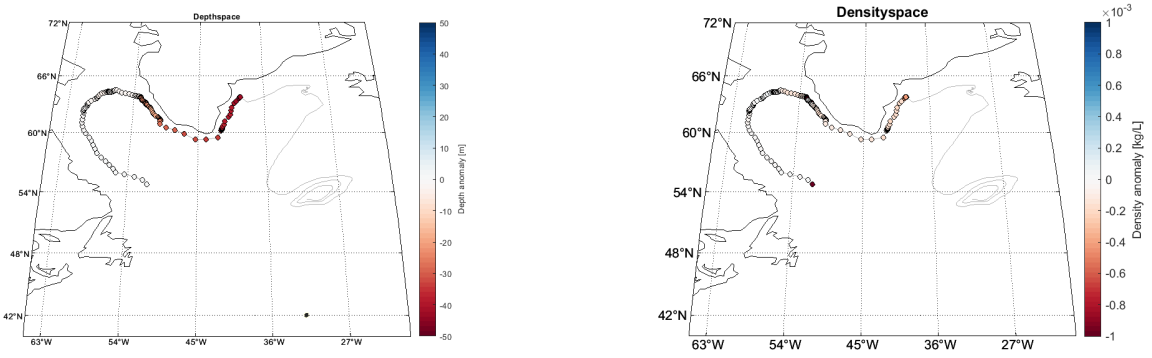

(a) (b)

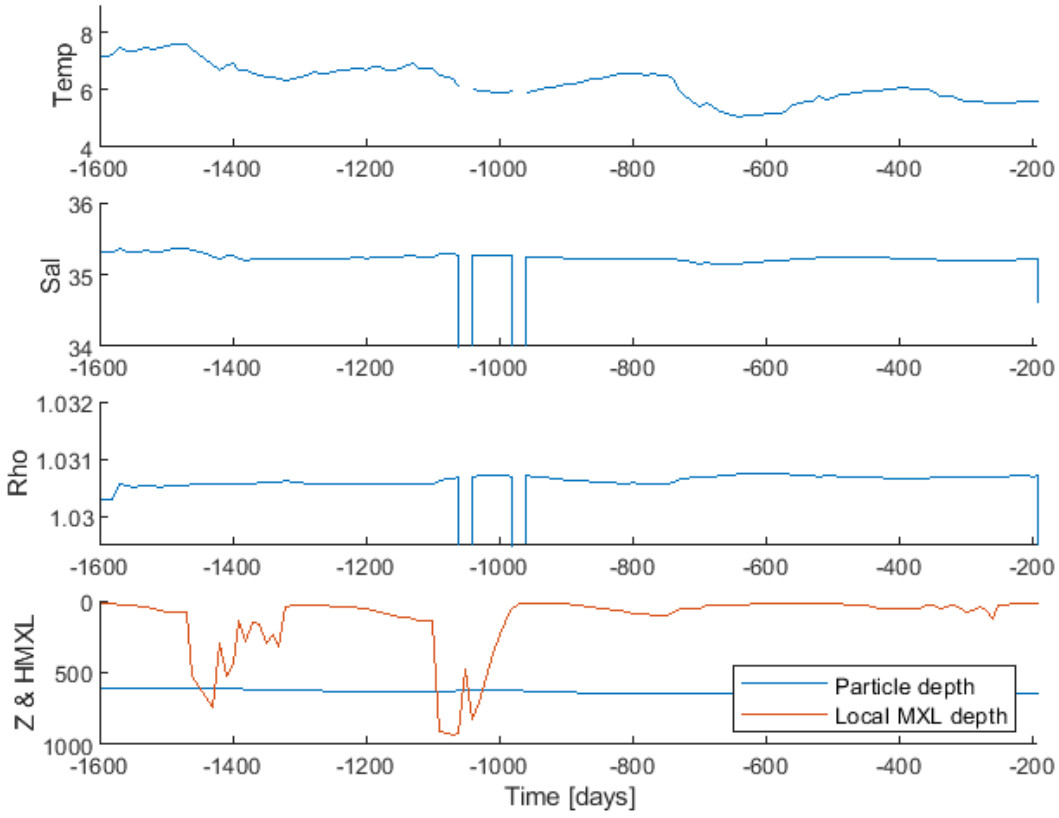

(c)

Figure 5.9: Example trajectory of overturning in depth space. The depth anomaly compared to the simulation start is plotted in (a), in (b) the density anomaly compared to the simulation start is plotted. (c) shows temperature, salinity and density over time as well as the depth together with the local mixed layer depth.

5.3. Summary

This chapter presented the analysis of the piControl simulation. First the mixed layer depths and the vertical velocities were analysed. Where the mixed layers, that reach a maximum of 1661 meter in March, are located in locations that are also found in other ocean models, their magnitude is smaller when compared to other models. Still, the depth of 1661 meter is deep enough to have the convection process reach depths at which LSW is usually found.

The strongest vertical velocities in the piControl simulation were found over the steep continental slopes, especially the slopes east and west of Greenland. These vertical velocities also have a strong seasonality. This seasonality was, following Equation 5.1, due to horizontal density differences. The locations of the vertical velocities, over the continental slope is what was expected for a system with sinking in a boundary current.

However, the Lagrangian analysis showed that there is not such a system, with a boundary current and an interior, in the CESM model. This has implications for the AMOC, because of the coarse grid resolution, an exchange mechanism bringing convected waters to the boundary using mesoscale eddies, is not present in the model. This reflected on the analysis of a few particle trajectories. The Lagrangian analysis showed that overturning in density space, the transformation of the particle properties due to convection, and the overturning in depthspace, the sinking of the particle, are two separate processes, which can occur separately of each other, due to the missing of an exchange mechanism.

The particle trajectories furthermore revealed that the ocean dynamics have a very viscous character. There is apparently a limited exchange between the subpolar and subtropical gyres and only few particles left the subpolar gyre through the Hudson-, Davis-, or Denmark Strait.

6

Analysing the 1pctCO2 simulation

This chapter analyses the 1pctCO2 simulation. As described in Section 3.1.2, the data used for this analysis is model year 330. For the first 140 years of the simulation, the CO_2 concentration in the atmosphere has been increased with 1% per year, until four times the initial concentration was reached in the year 140. After that, the concentration has been kept constant for the rest of the simulation. Following the approach of Chapter 4, first the mixed layers and the vertical velocities are analysed. However, since the structure of the AMOC in this simulation has changed completely, no Lagrangian analysis is performed. Instead, the temperature, salinity and density in this simulation are compared to the temperature, salinity and density in the piControl simulation.

6.1. Mixed layers and vertical velocities in the 1pctCO2 simulation

Figure 3.4 already showed that for the 1pctCO2 simulation, the AMOC strength is strongly reduced during the increase of the CO_2 concentrations. After model year 140, the concentrations are kept constant again and the AMOC strength stabilizes at a magnitude of approximately 5 Sv. Both Figures 3.4 and 4.1 indicate that the overturning is strongly reduced, but has not completely disappeared. Figure 6.1 shows the mixed layers north of the equator during February. It can be seen that deep mixed layers are no longer present in the subpolar North Atlantic. As can be seen in the figure, the mixed layers in the subpolar North Atlantic are very shallow, with a maximum in the Labrador Sea of 112 meter (area outlined by the dashed line in Figure 6.1). Figure 3.4 showed that the mixed layer depth in the Irminger Sea and Nordic Seas is in the same order of magnitude. And thus, deep convection in the subpolar North Atlantic has shut down.

Where the deep mixed layers in the subpolar North Atlantic have disappeared, deep mixed layers have emerged between $30°N$ and $40°N$. In Figure 6.1 are two areas with deeper mixed layers visible: one close to the American coast and one located further east, around $60°\ W$. The maximum mixed layer depth of 567 meter is located in the area close to the coast. This maximum depth is much shallower than the maximum in the piControl simulation, but it is a factor 5 deeper than the maximum mixed layer depth in the subpolar North Atlantic in the 1pctCO2 simulation. The latitudes where these deep mixed layers have emerged correspond to where the overturning streamfunction of Figure 4.1 has its maximum (north of $28°N$). In addition to this, the maximum of the overturning streamfunction has also become shallower.

Figure 6.2 shows the meridional velocities in a cross-section at $54,74°\ N$ in January of the 1pctCO2 simulation. Figure 6.2 shows that circulation in the subpolar gyre has been reduced. The velocities are smaller and concentrated in the upper part of the watercolumn. A DWBC similar to what is seen in Figure 4.2 is no longer to be present in the model.

Similar to the meridional velocities, have also the vertical velocities declined in magnitude in the 1pctCO2 simulation. Figure 6.3 shows the vertical velocities north of the equator at 500 meter depth. This depth is taken as Figure 4.1 indicates that the maximum of the overturning streamfunction, and thus the maximum vertical transport, can be found at approximately this depth. Note that almost all the vertical velocities in Figure 6.3 fall within the range of the used colorbar. One exception is the particular strong upwelling cell at $35°\ N$, with velocities of approximately 0.01 cm/s, next to the contour line of the deep mixed layers.

North of $45°\ N$ there is now a mixture of both up- and downwelling in the open ocean.

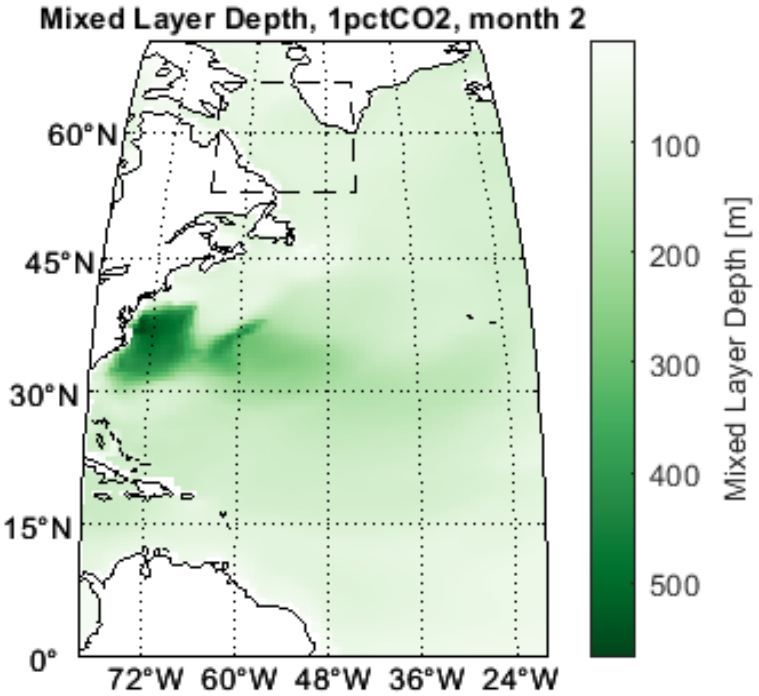

Figure 6.1: Mixed Layer Depths north of the equator for the 1pctCO2 simulation. The frame marks the area over which the maximum mixed layer in the Labrador Sea has been determined.

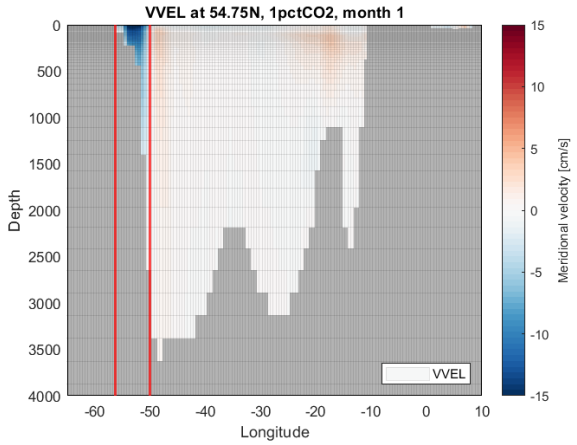

Figure 6.2: Cross-section of the meridional velocities at $54,75^{\circ}$ N, during January in the 1pctCO2 simulation

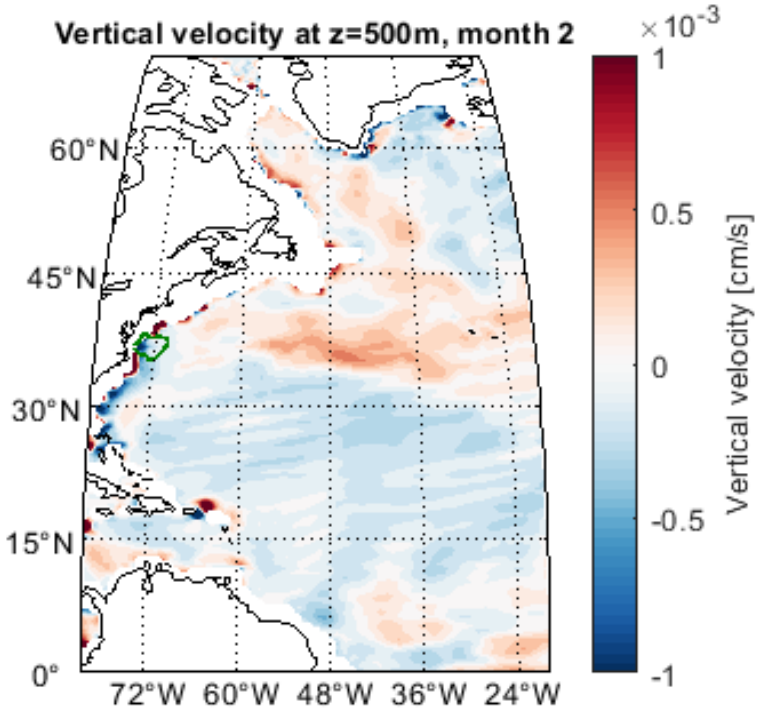

Figure 6.3: Vertical velocities at 500 meter depth in the 1pctCO2 simulation, with the 500m contour of the mixed layers indicated in green.

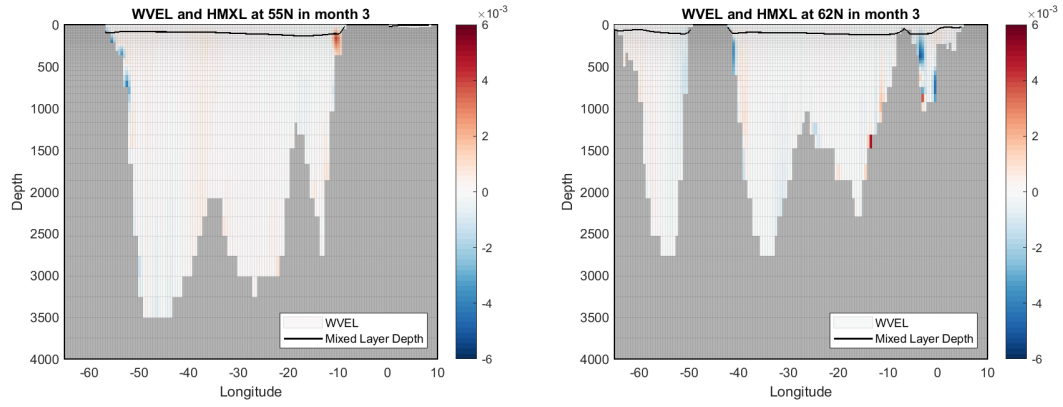

(a) (b)

Figure 6.4: Cross-sections of the vertical velocities at (a) 54.75° N and (b) 61.75° N, with the mixed layer depth indicated in black. Please note the scale differences compared to Figure 5.3

In the subpolar North Atlantic, downwelling can still be found on the steep continental slopes near Greenland. The strongest velocities are now on the eastern side of Greenland. On the other side of the Labrador Sea, near the Labrador coast, now mostly upwelling can be found, in contrast to the situation in the piControl simulation (see Figure 5.2). Both this up- and downwelling in the Labrador Sea are likely to be part of the cyclonic cell that can be seen in the overturning streamfunction. Further south, between 30° N and 45° N, are larger vertical velocities found over the continental slope. The particular strong upwelling cell next to the mixed layers has already been noted earlier in this section. To the North and South of this upwelling cell is there both up- and downwelling in this region.

From the cross-sections of Figure 6.4, it can be seen that these larger velocities are now only found in the upper few hundred meters of the watercolumn, while in the piControl simulation, these velocities reached depths of 2000 meters and more (see Figure 5.3). Figure 6.4 also shows the shallow mixed layers along these cross-sections. The shallow mixed layers indicate that deep convection has shut down.

6.2. Changes between the 1pctCO2 and piControl simulations

A possible explanation why the convection in the subpolar North Atlantic has shut down in the 1pctCO2 simulation is revealed by looking at the distribution of temperature, salinity and density. Figure 6.5 shows the differences between the 1pctCO2 simulation and the piControl simulation for temperature, salinity and density. Figure 6.5a shows the temperature differences. In particular in the subtropics, but also at mid-depths in the Labrador Sea, the ocean has warmed, in the order of about 10°C in the Labrador Sea. However, at the surface and near the bottom of the Labrador Sea, the change in temperature is limited. Figure 6.5b shows that a layer of fresher water has formed at the surface of the Labrador Sea. Below the fresh layer at the surface, the salinity has slightly increased, which contributes to a sharper halocline.

The small changes in temperature in this surface layer, in combination with the much fresher water, cause a strong reduction in the waters density in this surface layer (see Figure 6.5c). Outside of the Labrador Sea, the combination of a much warmer upper 2000 meter and only a small increase in salinity cause a small decrease in the waters density, although, this is decrease is about 5 times weaker than the decrease in density in the surface layer of the Labrador Sea.

The increased contrast in watermass properties between the surface layer and the rest of the upper ocean does not contribute to the convection process. Most likely, the atmospheric cooling at the surface is no longer able to create such dense waters that mixed layers can reach deeper than the surface layer. As can be seen in Figure 6.6, is it not only the upper ocean that has increased temperatures. Figure 6.6 (From Muntjewerf et al., 2020) shows the difference in mean near-surface temperature between the end of the 1pctCO2 simulation and the piControl simulation in Kelvin. Globally the near-surface temperatures have risen by about 10 K, which has definitely an impact on the way the ocean is cooled; for the cooling of the ocean surface in the Labrador Sea, but also further south, at the location of the new mixed layers.

Figure 6.7 shows the variability in temperature, salinity and density at the location of the deepest mixed layers, at (73.75°W,36.75°N). The figure shows the variability in the upper 700 meters of the watercolumn, together with the local mixed layer depth. Even though both the upper ocean and near-surface atmospheric temperatures have risen, remains atmospheric cooling the dominant process (e.g. between January and February there is a reduction 0.11 psu in surface salinity). Apparently, the ocean salinity does play an role in the convection process, as the freshwater input during May and June abruptly restratifies the ocean again.

What this analysis does not show, is how the dense waters spread out after convection. The framework (Spall and Pickart, 2001; Straneo, 2006) of sinking and densification along the boundary were derived for the situation of a boundary current circling a marginal sea with convection in the interior. In the current location, there is the Gulf Stream flowing along the shore in this region. It remains unclear if there is a densification over the boundary current, if the deep mixed layers are connected to sinking along the boundary in this region, especially as there is strong upwelling close to the mixed layers, and how this connection would look like.

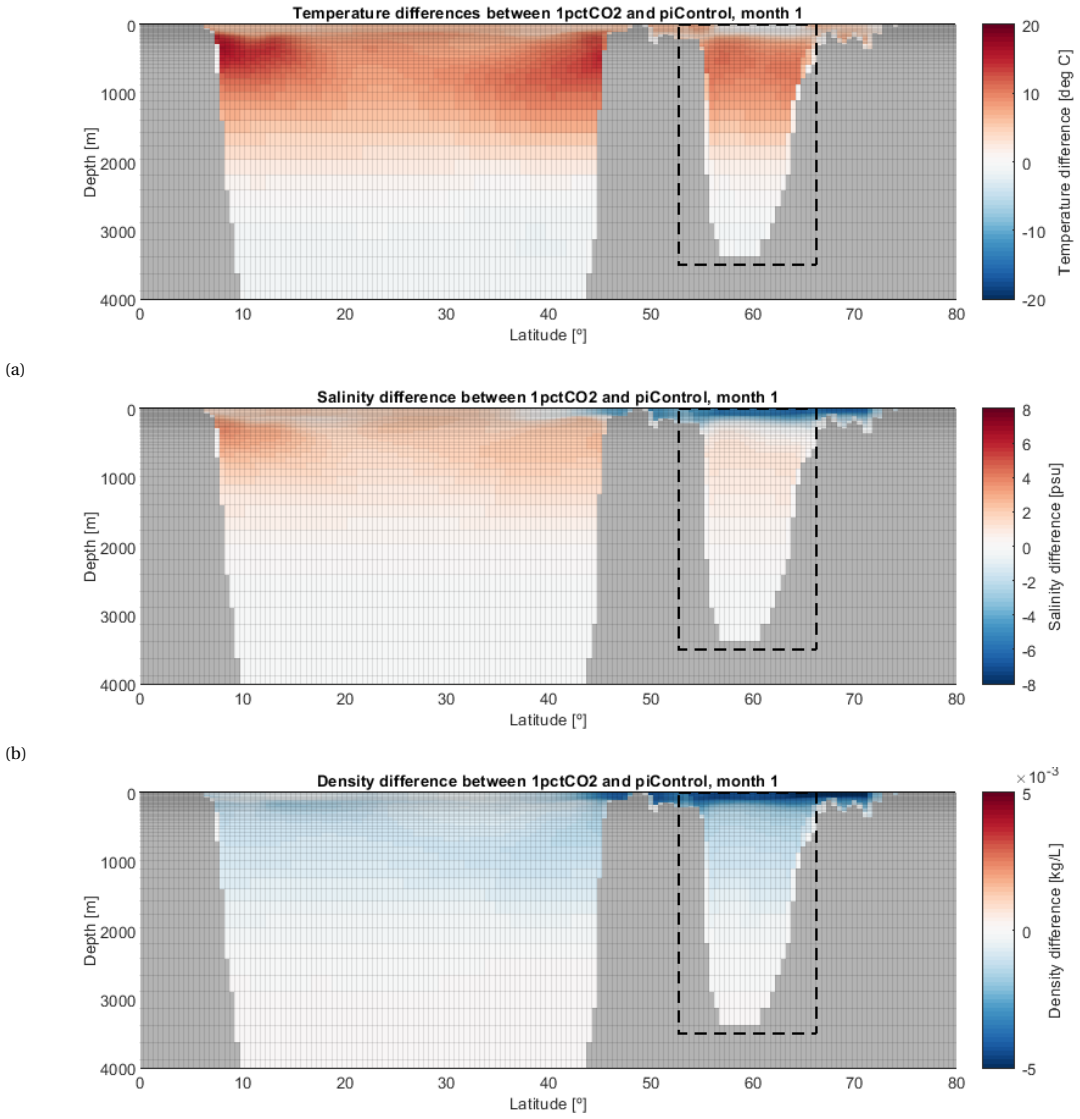

Figure 6.5: The differences between the 1pctCO2 simulation and the piControl simulation for (a) temperature, (b) salinity and (c) density. The cross-sections are taken at $55^{\circ}W$. The frame in the figures marks the Labrador Sea.

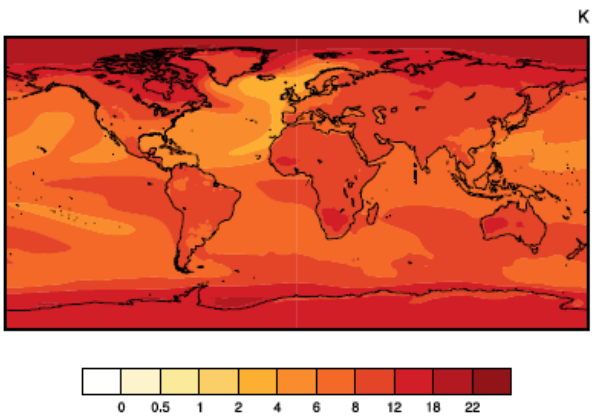

Figure 6.6: The near-surface temperature anomaly in Kelvin between model years 331-350 of the 1pctCO2 simulation and the piControl simulation (From Muntjewerf et al., 2020, their Figure 1.d).

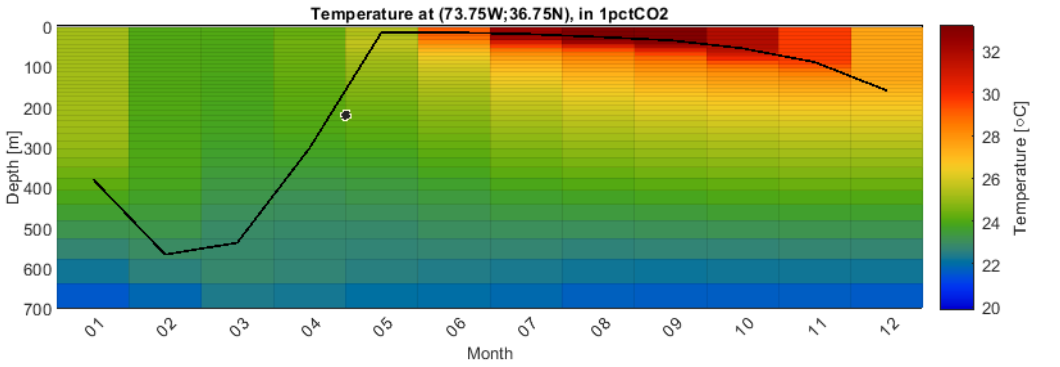

(a)

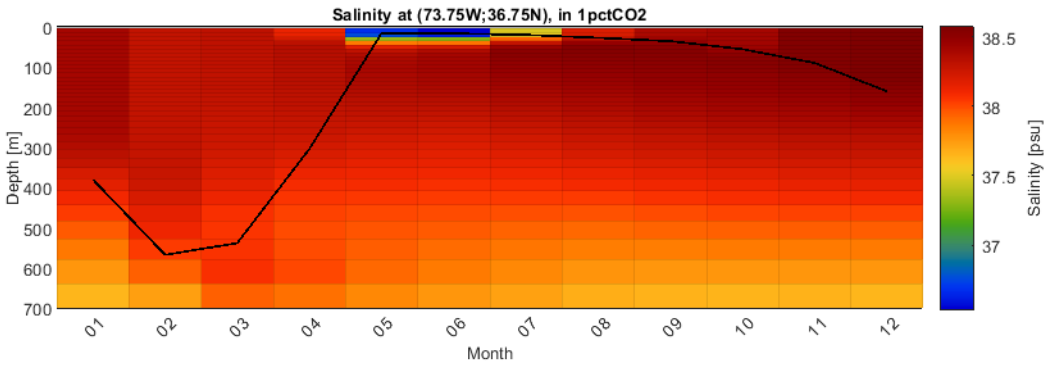

(b)

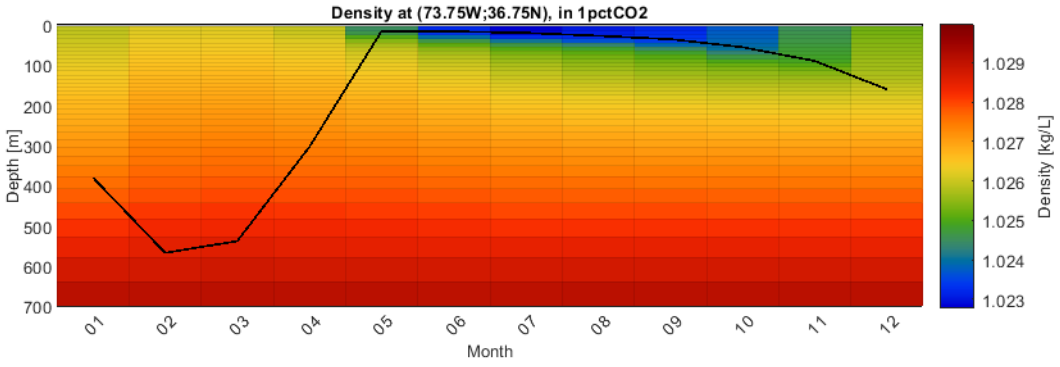

(c)

Figure 6.7: Variability of (a) temperature, (b) salinity and (c) density over time at (73.75W,36.75N) in the 1pctCO2 simulation. The local mixed layer depth is indicated by the black line.

6.3. Summary

This chapter analysed how the AMOC components have changed under rising CO_2 concentrations in the atmosphere, which has caused a strong reduction in AMOC strength. It showed that deep mixed layers have disappeared from the subpolar North Atlantic, and deep convection in this region has shut down. Instead new deep mixed layers have emerged between 30° N and 40° N. The maximum of these mixed layers is 550 meters. This depth is much shallower than the maximum that was found in the analysis of the piControl simulation.

In the 1pctCO2 simulation, the magnitude of the vertical velocities in the subpolar North Atlantic has declined. Compared to the piControl simulation, there is now a mixed pattern of both up- and downwelling in the open ocean. Larger vertical velocities are still found over the continental slopes, which is in line with Equation 5.1. There is also a particular strong upwelling cell located close to the deep mixed layers, but most of the continental slopes near the deep mixed layers have downwelling.

A possible explanation why the deep convection has shut down in the subpolar North Atlantic was presented by looking at the differences in temperature, salinity and density between the piControl simulation and the 1pctCO2 simulation. It showed that a new fresher layer has formed at the surface of the Labrador Sea. In general, the upper 2000 meter of the ocean has warmed significantly compared to the piControl simulation, with an exception for the new surface layer in the Labrador Sea. The temperature of this surface layer in the interior of the Labrador Sea has mostly stayed the same, but there is some warming over the continental shelves. The increased differences between the temperature and salinity of the new surface layer and the waters below has sharpened the thermo- and haloclines. Most likely, the atmospheric cooling at the surface is no longer able to create sufficiently dense waters that mixed layers can reach deeper than the surface layer.

7

Conclusion and discussion

This study analysed the characteristics of the AMOC in the CESM model. It also analysed the changes of the characteristics of the AMOC in response to rising concentrations of greenhouse gases in the atmosphere. For this, the data of two simulations was used. The first simulation is a reference run that aims to simulate the conditions prior to the Industrial Revolution. This so-called piControl simulation was analysed using both a Eulerian and a Lagrangian approach to get insight in how the characteristics of the AMOC are represented in the CESM model and how the pathways of the different watermasses associated with the AMOC are connected.

In the second simulation used for this study, the CO_2 concentrations in the atmosphere were increased linearly for a duration of 140 years. After 140 years, the concentration was kept constant for the rest of the simulation. The data used was modelyear 330 of this 1pctCO2 simulation. This 1pctCO2 simulation was used to analyse the change of the AMOC characteristics in comparison to the characteristics in the piControl simulation.

The data of these two simulations was used to find an answer to the main research question;

Does the decline in AMOC strength in response to increasing atmospheric greenhouse gas concentrations in a low resolution climate model like CESM constitute a reliable climate projection, considering our knowledge of AMOC dynamics?

And for the following subquestions;

- Are the characteristics of the AMOC (overturning strength, spatial distributions of convection and downwelling) as simulated by the CESM model in agreement with the current knowledge based on literature and in particular on that deduced from higher resolution models?
- How are the convection regions connected to the downwelling regions?
- How do the characteristics of the AMOC in the subpolar North Atlantic Ocean change in the CESM model in response to rising CO_2 concentrations in the atmosphere?

These subquestions will be answered first, before the main research question will be addressed.

Are the characteristics of the AMOC (overturning strength, spatial distributions of convection and downwelling) as simulated by the CESM model in agreement with the current knowledge based on literature and in particular on that deduced from higher resolution models?

The first subquestion looked into the characteristics of the AMOC in the CESM model and compared these to the current knowledge from literature and higher resolution ocean models. One indicator of a model's ability to represent the AMOC in a reasonable sense, is the AMOC strength. The AMOC strength is most often defined as the maximum of the overturning streamfunction, north of a certain latitude. For the strength of the AMOC in the CESM model, the overturning streamfunction was defined as north of 28° N and below 500 meter depth

(Muntjewerf et al., 2020). For the piControl simulation, it amounts to approximately 24 Sv. This AMOC strength in the piControl simulation is comparable to what is found in other climate models participating in CMIP6 and from observational arrays (Weijer et al., 2020). It is also comparable to ocean-only models (e.g. Sayol et al., 2019).

That the AMOC strength is comparable to other models and data is a reflection of the representation of the different components of the AMOC in the model. Literature (e.g. Katsman et al., 2018, and references therein) shows that the overturning process can be characterised by two different components. First the water masses are transformed, this happens during (deep) convection. The second component is the sinking of the water to larger depths. An indicator for convection in the model is the presence of deep mixed layers. In the CESM model, these are found in the marginal seas of the subpolar North Atlantic. The deepest mixed layers have a maximum of 1661 meter and are found in the Labrador Sea, close to the West-Greenland coast. The location of the deep mixed layers in the CESM model is similar to the location of deep mixed layers in a coarse resolution ocean-only model (Katsman et al., 2018), but in higher resolution models and observations, the deepest mixed layers are found more centrally in the interior of the Labrador Sea (Georgiou et al., 2020a; Katsman et al., 2018; Pickart et al., 2002). The maximum of the CESM model is shallower than the what is found in both the ocean-only models of Katsman et al. (2018), in which the deep mixed layers reach to depths between 2000 and 3000 meter. When compared to the observations of Pickart et al. (2002), who found mixed layers up to 1400 meter, are the mixed layers in the CESM model a bit deeper.

The second component of the AMOC is the sinking of the convected waters to larger depths. According to literature and modelling studies (e.g. Katsman et al., 2018; Sayol et al., 2019), the downwelling part of the AMOC occurs mostly in the boundary current, which flows around the marginal seas of the northern Atlantic. Spall and Pickart (2001) showed that the vertical velocities in the boundary current are the effect of alongshore horizontal density differences. In the CESM model, stronger vertical velocities were indeed found along the continental slopes in the model. The strongest vertical velocities were found in around Greenland. These maxima were found at a depth of 1000 meter, which corresponds to the depth at which the overturning streamfunction has its maximum.

The AMOC strength in the CESM model is comparable to other climate models, ocean-only models and observations. Also the downwelling can be found in similar locations as in other ocean-only models. The mixed layer depths in the CESM model are shallower than what is found in the ORCA ocean-only model of Katsman et al. (2018). The mixed layers in the CESM model are located closer to the West-Greenland coast. A similar location is also seen in a 1° ocean-only model, while in higher resolution models, the deep mixed layers are found more centrally in the Labrador Sea. In conclusion, the CESM model has a good representation of the convection and the time-mean downwelling in the subpolar North Atlantic.

How are the convection regions connected to the downwelling regions?

Modelling studies (e.g. Georgiou et al., 2019) showed the importance of mesoscale eddies in the exchange of convected water between the interior of the sea and the boundary current, where most of the downwelling occurs. However, due to the coarse, 1° resolution grid, such mesoscales eddies cannot be resolved in the model. These eddies are parametrized as a subgrid scale process and thus, the exchange of waters between the interior and boundary, as caused by these eddies, is expected to be absent in the CESM model. Which has as consequences that convected waters remain as a stagnant pool in the convection region, or that convected waters are advected, but not being downwelled in the model.

In order to visualize a possible connection between the convection areas and the downwelling areas, Lagrangian particle tracking was performed. Particles were seeded in the ocean at a monthly interval during the first year of the simulation. The backward simulation traced the particles during 15 years of simulation. The forward simulation traced the particles during 10 years of simulation. This particle tracking first revealed that there is in fact only a limited exchange between the subpolar and subtropical gyres and through the Hudson-, Davis- and Denmark Strait. Only a few particles had a trajectory going throught the Hudson-, Davis- or Denmark Strait. Furthermore, apparently there is only one export pathway for particles out of the subpolar gyre to the subtropical gyre. This pathway is on the eastern side of the Atlantic Ocean, which suggest that the particles are being blocked by the NAC.

In higher resolution models, convected water from the interior leaves the sea through the boundary current, with mesoscale eddies playing an important role in the exchange between the interior and the boundary (Georgiou et al., 2020a). The particle tracking in the CESM showed that the particles move more as a very viscous flow through the model. Instead of displaying multiple different pathways and exchanges through the

boundary current and the interior of the sea, does this pathway cross the interior of the Labrador Sea. Apparently the parametrization of the mesoscale eddies caused the physical exchange between the convection region and the boundary current to be absent. So the particles have to be in the right place at the right time in order to experience convection. Otherwise, they flow through the area without convection, or with only downwelling when the trajectory is close to the continental slope. The trajectories of some example particles showed that most of the particles either have only convection or only downwelling. But that the combination of both, as in the total overturning process, only happens in a few occassions.

The way mesoscale eddies are parametrized has effect on the model, it contributes to the presence of the mixed layers and on the density differences along the boundary, but it does not contribute to the exchange between the interior and boundary. This Lagrangian analysis showed that the streamfunctions as often found in literature are mostly an indicator for the downwelling component of the overturning, but not an indicator for the overturning of convected waters. Convected waters can be downwelled, when the convection happens close to the boundary, however, since the convection is mostly located in the open ocean, this is more often not the case. So the AMOC is not only determined by the overturning strength. The AMOC is the combination of both convection and downwelling. Therefore, care should be taken by basing conclusions on only the AMOC strength, as depicted by the overturning streamfunction.

How do the characteristics of the AMOC in the subpolar North Atlantic Ocean change in the CESM model in response to rising CO_2 concentrations in the atmosphere?

For the 1pctCO2 simulation, Figure 3.4 revealed a steady decline in the AMOC strength during the increase of the CO_2 concentrations in the atmosphere. The AMOC strength stabilized at approximately 5 Sv after the concentrations were kept constant for the remainder of the simulation. The overturning streamfunction also showed that the location where the maximum occurs has moved to the south, and has become shallower. In the 1pctCO2 simulation, deep mixed layers have disappeared from the subpolar North Atlantic, and deep convection has completely stopped. Instead, deep mixed layers have emerged further to the south, between 30° N and 40° N, where mixed layers are found with a maximum of approximately 550 meter. In the 1pctCO2 simulation, the vertical velocities have declined in magnitude, both in the open ocean and over the continental slopes. Still, larger velocities are found over the continental slopes compared to the continental slopes. The largest vertical velocities are found close to deep mixed layers, with both strong up- and downwelling cells. Even though both the upper ocean and near-surface atmospheric temperatures have risen, remains temperature-driven convection the dominant convection process. The connection of the convected waters to the boundary and downwelling between 30° and 40°N remains unclear.

A closer look at the Labrador Sea in the 1pctCO2 revealed a possible explanation for the shutdown of deep convection in this area. At the surface, a layer of fresh water has formed, most likely a product of increased melting in the Arctic and runoff of the Greenland Ice Sheet. Below this layer of fresh water, the Labrador Sea has warmed and it has become more saline. Both the increase in temperature and salinity have created a strong thermo- and halocline at the bottom of this fresh surface layer. This is probably prohibiting convection from reaching larger depths.

In conclusion, the overturning strength in of the AMOC in the 1pctCO2 simulation is strongly reduced, as a result of much weaker vertical velocities in the model. Convection in the subpolar North Atlantic has shut down, as a new fresh surface layer has formed in the Labrador Sea, which prevents the development of deep mixed layers. In the 1pctCO2 simulation, new deep mixed layers have emerged further south in the model, beteen 30° N and 40° N. It remains unclear how these are connected to a downwelling location in the model.

Main research question: Does the decline in AMOC strength in response to increasing atmospheric greenhouse gas concentrations in a low resolution climate model like CESM constitute a reliable climate projection, considering our knowledge of AMOC dynamics?

It has been shown that CESM model can reproduce the two main components of the AMOC reasonably well in the piControl simulation. Both the convection and the downwelling are present in the model at the locations and with the magnitudes that are expected. The Lagrangian analysis showed that in this CESM model with a coarse 1° grid, the exchange mechanism between the convection and downwelling, in the form of mesoscale eddies, cannot be resolved. Instead of moving through a system with a boundary current and an interior, did the particles behave as a very viscous flow and they crossed the Labrador Sea rather than moving along the boundary.

This study emphasized that an overturning streamfunction simplifies the complexity of the overturning process. The streamfunction is a measure for the overturning strength, but is does not take into account how and if, the convection process and the exchange between convection and downwelling are represented. Care should therefore be taken when basing conclusions on the overturning streamfunction, as a good representation of the AMOC strength does not show if the overturning in density space and the connection between depth and density space are represented equally well.

The analysis of the 1pctCO2 simulation showed that deep convection has shut down in subpolar North Atlantic, but deep mixed layers have emerged further south. The piControl simulation showed that the CESM model can reproduce the physics of the two AMOC components, convection and downwelling, reasonably well, but the connection between overturning in density and depth space is missing. The new location of the mixed layers makes it questionable if the connection between convection and downwelling is still controlled by the same physics, since the convection has moved from a marginal sea to the open ocean and the CESM model cannot reproduce the connection between convection and downwelling. Climate projections based on simulations like the 1pctCO2 simulation would lose their reliability when other physical processes can come into play as a result of the changed climate or when the structure of the AMOC becomes different than it is in the present state, as in that case, the piControl simulation is no longer an indicator how well the processes are represented.

8

Recommendations

This thesis presented an analysis of the AMOC components in both the piControl simulation and after an increase of the atmospheric CO_2 concentrations, the 1pctCO2 simulations. In this chapter, a few recommendations for future work are given. This include both recommendations to improve on the used techniques, as well as some areas that deserve additional interest.

Chapter 5 presented the analysis of the piControl simulation. In this analysis a Lagrangian approach was used, using Parcels. Section 3.3 indicated that the use of this software, in combination with the coarse grid of the model, did not work perfectly. A lot of the particles got stuck in the steep bathymetry of the Labrador Sea, resulting in a loss of particles and hiatus in the storing of the tracer values. Section 3.3 showed the random movement kernel that was applied in an attempt to prevent the particles from getting stuck. It saved some particles from being stuck, but the particles would still have gaps in the stored tracer values. For future research, it is advised to use a much smaller timestep for the advection of the particles. This might help in preventing the particles from getting stuck in the bathymetry, and together with a much larger particleset, does it open up opportunities for additional analysis. For example using statistical and probabilistic analysis.

Furthermore, the ocean circulation in the piControl simulation can be further investigated. The Lagrangian particle tracking indicated a very limited exchange between the subpolar gyre and for example the Nordic Seas, and only a single export pathway for the particles from the Labrador Sea to the subtropical gyre. First, for the connection between the subpolar gyre and the Nordic Seas. To enter or leave the Nordic Seas, the water has to cross either the Denmark Strait or cross the Iceland-Scotland overflow. The forward tracing of particles in Figure 5.6 shows that more particles go in this direction than in Figure 5.5, in which the particles are traced backwards. The forward simulation follows the upper limb of the AMOC, while the backwards simulation came from the lower limb. A closer look at the pathways of the particles near the overflow regions might shed a light on why there is such a limited exchange over the overflows. Second, the export pathways from the Labrador Sea to the subtropical gyre. Section 2.3 indicated multiple pathways out of the subpolar North Atlantic. Besides the option to flow into the Irminger Sea, are the options for example follow the DWBC further south, to flow south along either side of the Mid-Atlantic Ridge or the pathway that is indicated in Figure 5.6, first to cross the Atlantic Ocean before flowing south. The figure suggests that the NAC might play an important role in preventing the transport to the subtropical gyre by blocking the particles. Only on the eastern side of the Atlantic, where the flow of the NAC has weakened seems it to be possible for the particles to find a pathway south. Is it only the NAC, and thus the ocean circulation in the model, that cause the limited exchange between the subpolar and subtropical gyres, or that other factors have an influence as well can be furhter investigated. This can be investigated by seeding for example particles in suspected pathways on the other side of the NAC and tracing them backwards. Also, a Eulerian view might contribute to the answer by for example showing how deep the NAC extends.

Chapter 6 analysed the change of the AMOC components after the increase of the atmospheric CO_2 concentrations in the atmosphere. A tremendous change in the AMOC behaviour was, based on Figures 3.4 and 4.1, to be expected. Further research can be done on what drives the connection between the convection region and sinking location. Higher resolution models have shown that eddies shed from the boundary current play an important role in the connection between convection and sinking, but it is unclear if these would be present in

the new location as well. This needs to be researched using Lagrangian methods in a higher resolution model, as the CESM model cannot reproduce the connection on the current grid.

Another question that can be asked for the 1pctCO2 simulation, is if the overturning process displays the same relation between convection and downwelling. The convection in the open ocean might be different compared to the convection in a marginal sea, where the boundary current circles the convection region. The overturning near the boundary in Equation 5.1 depends on horizontal alongshore density changes, or in other words, a densification along the boundary current. It can be investigated if this is also the case along the boundaries near the new mixed layers, especially since there are also strong upwelling cells present near these mixed layers.

The two simulations used in this study are each at an other end of the spectrum. The piControl simulation served as a reference run for the present day. While the 1pctCO2 simulation was the last part of the simulation in which the CO_2 concentrations have risen. Chapter 6 showed that the changes between the 1pctCO2 simulation and the piControl simulation are very large, for the spatial distributions of the AMOC as well as for the temperature, salinity and density of the ocean in general. To get a better understanding on how the AMOC developed this way, also the transient state between the piControl simulation and 1pctCO2 simulation can be looked at. During the first 140 years of the 1pctCO2 simulation, the atmospheric CO_2 concentrations are being increased. As can be seen in Figure 3.4, does there occur a sudden collapse of the mixed layer depths in the subpolar North Atlantic, around model year 50 in the case of the Labrador Sea. One or multiple periods during these first 140 years of the 1pctCO2 simulation can be analysed to see how the transition between the AMOC state in the piControl simulation develops into the AMOC state by the end of the 1pctCO2 simulation.

When Lagrangian particle tracking is used for the analysis of a transient state, one needs to take care. The state of the AMOC is changing during the advection of the particles, and thus, particles released during the first year, might behave completely different compared to particles released in the last year of the simulation. In this study, particles were only released during the first year, on a monthly interval. For an analysis of the transient state, it is recommended to release particle throughout the entire simulation period. Furthermore, in a transient state of the model, is it most likely that the last month of a model year does not seamlessly connect to the first year of said model year. Therefore, looping of the data to reduce the data-input, as was done in this study, is not recommended. Instead, the data of all the years analysed in the Lagrangian particle tracking need to be used as input for the particle tracking software.

Bibliography

M. Bollmann, T. Bosch, F. Colijn, R. Ebinghaus, R. Froese, K. Güssow, S. Khalilian, S. Krastel, A. Körtzinger, M. Langenbuch, M. Latif, B. Matthiessen, F. Melzner, A. Oschlies, S. Petersen, A. Proelß, M. Quaas, J. Reichenbach, T. Requate, T. Reusch, P. Rosenstiel, J. O. Schmidt, K. Schrottke, H. Sichelschmidt, U. Siebert, R. Soltwedel, U. Sommer, K. Stattegger, H. Sterr, R. Sturm, T. Treude, A. Vafeidis, C. Van Bernem, J. Van Beusekom, R. Voss, M. Visbeck, M. Wahl, K. Wallman, and F. Weinberger. World Ocean Review, Living with the oceans. maribus gGmbH, 2010. ISBN 9783866480124.

A. Bower, S. Lozier, and S. Gary. Export of Labrador Sea Water from the subpolar North Atlantic: A Lagrangian perspective. Deep-Sea Research Part II: Topical Studies in Oceanography, 58(17-18):1798–1818, 2011. ISSN 09670645. doi: 10.1016/j.dsr2.2010.10.060. URL http://dx.doi.org/10.1016/j.dsr2.2010.10.060.

A. Bower, S. Lozier, A. Biastoch, K. Drouin, N. Foukal, H. Furey, M. Lankhorst, S. Rühs, and S. Zou. Lagrangian Views of the Pathways of the Atlantic Meridional Overturning Circulation. Journal of Geophysical Research : Oceans, 124:5313–5335, 2019. doi: 10.1029/2019JC015014. URL https://doi.org/10.1029/2019JC015014.

W. Broecker. The Great Ocean Conveyor. Oceanography, 4(2):79–89, 1991. ISSN 10428275. doi: 10.5670/oceanog.1991.07.

N. Brüggemann and C. A. Katsman. Dynamics of Downwelling in an Eddying Marginal Sea : Contrasting the Eulerian and the Isopycnal Perspective. Journal of Physical Oceanography, 49:3017–3035, 2019. doi: 10.1175/JPO-D-19-0090.1.

J. L. Bullister, M. Rhein, and C. Mauritzen. Deepwater Formation. In International Geophysics, volume 103, chapter 10, pages 227–253. Elsevier Ltd., 2013. ISBN 9780123918512. doi: 10.1016/B978-0-12-391851-2.00010-6. URL http://dx.doi.org/10.1016/B978-0-12-391851-2.00010-6.

M. Collins, R. Knutti, J. Arblaster, J-L Dufresne, T. Fichefet, P. Friedlingstein, X. Gao, W. J. Gutowski, T. Johns, G. Krinner, M. Shongwe, C. Tebaldi, A. J. Weaver, and M. Wehner. Long-term Climate Change: Projections, Commitments and Irreversibility. In T. F. Stocker, D Qin, G-K Plattner, M Tignor, S K Allen, J Boschung, A Nauels, Y Xia, V Bex, and P M Midgley, editors, Climate Change 2013: The Physical Science Basis. Contribution of Working Group 1 to the Fifth Assessment Report of the Intergovernmental Panel on Climate Change, chapter 12. Cambridge University Press, Cambridge, UK and New York, USA, 2013.

B. Cushman-Roisin and J. M. Beckers. Introduction to Geophysical Fluid Dynamics, volume 101. Academic Press, 2011. ISBN 9780120887590. doi: 10.1016/B978-0-12-088759-0.00001-8.

G. Danabasoglu, S. C. Bates, B. P. Briegleb, S. R. Jayne, M. Jochum, W. G. Large, S. Peacock, and S. G. Yeager. The CCSM4 ocean component. Journal of Climate, 25, 2012. doi: 10.1175/JCLI-D-11-00091.1.

G. Danabasoglu, J. F. Lamarque, J. Bacmeister, D. A. Bailey, A. K. DuVivier, J. Edwards, L. K. Emmons, J. Fasullo, R. Garcia, A. Gettelman, C. Hannay, M. M. Holland, W. G. Large, P. H. Lauritzen, D. M. Lawrence, J. T.M. Lenaerts, K. Lindsay, W. H. Lipscomb, M. J. Mills, R. Neale, K. W. Oleson, B. Otto-Bliesner, A. S. Phillips, W. Sacks, S. Tilmes, L. van Kampenhout, M. Vertenstein, A. Bertini, J. Dennis, C. Deser, C. Fischer, B. Fox-Kemper, J. E. Kay, D. Kinnison, P. J. Kushner, V. E. Larson, M. C. Long, S. Mickelson, J. K. Moore, E. Nienhouse, L. Polvani, P. J. Rasch, and W. G. Strand. The Community Earth System Model Version 2 (CESM2). Journal of Advances in Modeling Earth Systems, 12, 2020. doi: 10.1029/2019MS001916.

M. F. de Jong and L. de Steur. Strong winter cooling over the Irminger Sea in winter 2014–2015, exceptional deep convection, and the emergence of anomalously low SST. Geophysical Research Letters, 43:7106–7113, 2016. ISSN 19448007. doi: 10.1002/2016GL069596.

M. F. De Jong, M. Oltmanns, J. Karstensen, and L. De Steur. Deep convection in the Irminger Sea observed with a dense mooring array. Oceanography, 31(1):50–59, 2018. ISSN 10428275. doi: 10.5670/oceanog.2018.109.

P. Delandmeter and E. Van Sebille. The Parcels v2.0 Lagrangian framework: New field interpolation schemes. Geoscientific Model Development, 12(8):3571–3584, 2019. ISSN 19919603. doi: 10.5194/gmd-12-3571-2019.

K. Döös. Interocean exchange of water masses. Journal of Geophysical Research, 100(C7):13499–13514, 1995. ISSN 01480227.

V. Eyring, S. Bony, G. A. Meehl, C. A. Senior, B. Stevens, R. J. Stouffer, and K. E. Taylor. Overview of the Coupled Model Intercomparison Project Phase 6 (CMIP6) experimental design and organization. Geoscientific Model Development, 9:1937–1958, 2016. doi: 10.5194/gmd-9-1937-2016.

R. Gelderloos, C. A. Katsman, and K. Våge. Detecting Labrador Sea Water formation from space. Journal of Geophysical Research: Oceans, 118:2074–2086, 2013. ISSN 21699291. doi: 10.1002/jgrc.20176.

P. R. Gent. Coupled models and climate projections. In Ocean Circulation and Climate: A 21st Century Perspective, volume 103, chapter 23, pages 609–623. Elsevier Ltd., 2013. ISBN 9780123918512. doi: 10.1016/B978-0-12-391851-2.00023-4. URL http://dx.doi.org/10.1016/B978-0-12-391851-2.00023-4.

S. Georgiou, C. G. van der Boog, N. Brüggemann, S. L. Ypma, J. D. Pietrzak, and C. A. Katsman. On the interplay between downwelling, deep convection and mesoscale eddies in the Labrador Sea. Ocean Modelling, 135 (August 2018):56–70, 2019. ISSN 14635003. doi: 10.1016/j.ocemod.2019.02.004.

S. Georgiou, S. L. Ypma, N. Brüggemann, C. G. Van Der Boog, P. Spence, J. D. Pietrzak, and C. A. Katsman. Direct and indirect pathways of convected water masses and their impacts on the overturning dynamics of the Labrador Sea. Journal of Geophysical Research: Oceans, pages 1–36, 2020a.

S. Georgiou, S. L. Ypma, N. Brüggemann, J. Sayol, J. D. Pietrzak, and C. A. Katsman. Pathways of the water masses exiting the Labrador Sea : The importance of boundary – interior exchanges. Ocean Modelling, 150: 101623, 2020b. ISSN 1463-5003. doi: 10.1016/j.ocemod.2020.101623. URL https://doi.org/10.1016/j.ocemod.2020.101623.

J. W. Hurrell, M. M. Holland, P. R. Gent, S. Ghan, J. E. Kay, P. J. Kushner, J.-F. Lamarque, W. G. Large, D. Lawrence, K. Lindsay, W. H. Lipscomb, M. C. Long, N. Manhowald, D. R. Marsh, R. B. Beale, P. Rasch, S. Vavrus, M. Verteinstein, D. Bader, W. D. Collins, J. J. Hack, J. Kiehl, and S. Marshall. The Community Earth System Model; A Framework for Collaborative Research. B. Am. Meteorol. Soc., 94(November 2012):1339–1360, 2013. doi: 10.1175.BAMS-D-12-00121.1.

IPCC. IPCC Special Report on the Ocean and Cryosphere in a Changing Climate, 2019.

C. A. Katsman, S. S. Drijfhout, H. A. Dijkstra, and M. A. Spall. Sinking of dense north atlantic waters in a global ocean model: Location and controls. Journal of Geophysical Research: Oceans, 123(5):3563–3576, 2018. ISSN 21699291. doi: 10.1029/2017JC013329.

W. H. Lipscomb, S. F. Price, M. J. Hoffman, G. R. Leguy, A. R. Bennett, S. L. Bradley, K. J. Evans, J. G. Fyke, J. H. Kennedy, M. Perego, D. M. Ranken, W. J. Sacks, A. G. Salinger, L. J. Vargo, and P. H. Worley. Description and evaluation of the Community Ice Sheet Model (CISM) v2.1. Geoscientific Model Development, 12(1):387–424, 2019. ISSN 19919603. doi: 10.5194/gmd-12-387-2019.

M. S. Lozier, S. Bacon, A. S. Bower, S. A. Cunningham, M. F. de Jong, L. de Steur, B. DeYoung, J. Fischer, S. F. Gary, B. J. W. Greenan, P. Heimbach, N. P. Holliday, L. Houpert, M. E. Inall, W. E. Johns, H. L. Johnson, J. Karstensen, F. Li, X. Lin, N. Mackay, D. P. Marshall, H. Mercier, P. G. Myers, R. S. Pickart, H. R. Pillar, F. Straneo, V. Thierry, R. A. Weller, R. G. Williams, C. Wilson, J. Yang, J. Zhao, and J. D. Zika. Overturning In The Subpolar North Atlantic Program; A New International Ocean Observing System. Bulletin of the American Meteorological Society, 98(4):737–752, 2017. doi: 10.1175/BAMS-D-16-0057.1.

G. D. McCarthy, D. A. Smeed, S. A. Cunningham, and C. D. Roberts. Atlantic Meridonal Overturning Circulation. MCCIP Science Review 2017, pages 1–7, 2017. doi: 10.14465/2017.arc10.002-atl. URL www.ncdc.noaa.gov.

E. G. Morozov, A. N. Demidov, R. Y. Tarakanov, and W. Zenk. Water Structure and Flows; Abyssal Channels of the Atlantic Ocean. Springer Dordrecht Heidelberg London New York, 2010. ISBN 978-90-481-9357-8. doi: 10.1007/978-90-481-9358-5.

L. Muntjewerf, R. Sellevold, M. Vizcaino, C. Ernani da Silva, M. Petrini, and K. Thayer-Calder. Accelerated greenland ice sheet mass loss under high greenhouse gas forcing as simulated by the coupled cesm2.1-cism2. Journal of Advances in Modeling Earth Systems, pages 1–40, 2020.

R. S. Pickart, D. J. Torres, and R. A. Clarke. Hydrography of the Labrador Sea during Active Convection. J. Phys. Oceangr., 32(2):428–457, 2002. doi: https://doi.org/10.1175/1520-0485(2002)032<0428:HOTLSD>2.0.CO;2.

J. Sayol, H. Dijkstra, and C. A. Katsman. Seasonal and regional variations of sinking in the subpolar North Atlantic from a high-resolution ocean model. Ocean Science, 15:1033–1053, 2019.

D. A. Smeed, G. D. McCarthy, S. A. Cunningham, E. Frajka-Williams, D. Rayner, W. E. Johns, C. S. Meinen, M. O. Baringer, B. I. Moat, A. Duchez, and H. L. Bryden. Observed decline of the Atlantic meridional overturning circulation 2004-2012. Ocean Science, 10:29–38, 2014. ISSN 18120784. doi: 10.5194/os-10-29-2014.

R. Smith, P. Jones, B. Briegleb, F. Bryan, G. Danabasoglu, J. Dennis, J. Dukowicz, C. Eden, B. Fox-Kemper, P. Gent, M. Hecht, S. Jayne, M. Jochum, W. Large, K. Lindsay, M. Maltrud, N. Norton, S. Peacock, M. Vertenstein, and S. Yeager. The Parallel Ocean Program (POP) Reference Manual. Technical report, Los Alamos National Laboratory, 2010.

M. A. Spall and R. S. Pickart. Where Does Dense Water Sink ? A Subpolar Gyre Example. Journal of Physical Oceanography, 31:810–826, 2001. doi: https://doi.org/10.1175/1520-0485(2001)031{\%}3C0810:WDDWSA{\%}3E2.0.CO;2.

F. Straneo. On the connection between dense water formation, overturning, and poleward heat transport in a convective basin. Journal of Physical Oceanography, 36:1822–1840, 2006. ISSN 00223670. doi: 10.1175/JPO2932.1.

E. van Sebille, S. M. Griffies, R. Abernathey, T. P. Adams, P. Berloff, A. Biastoch, B. Blanke, E. P. Chassignet, Y. Cheng, C. J. Cotter, E. Deleersnijder, K. Döös, H. F. Drake, S. Drijfhout, S. F. Gary, A. W. Heemink, J. Kjellsson, I. M. Koszalka, M. Lange, C. Lique, G. A. MacGilchrist, R. Marsh, C. G. Mayorga Adame, R. McAdam, F. Nencioli, Cl. B. Paris, M. D. Piggott, J. A. Polton, S. Rühs, S. H. A. M. Shah, M. D. Thomas, J. Wang, P. J. Wolfram, L. Zanna, and J. D. Zika. Lagrangian ocean analysis: Fundamentals and practices. Ocean Modelling, 121(October 2017):49–75, 2018. ISSN 14635003. doi: 10.1016/j.ocemod.2017.11.008.

W. Weijer, W. Cheng, O. A. Garuba, A. Hu, and B. T. Nadiga. CMIP6 Models Predict Significant 21st Century Decline of the Atlantic Meridional Overturning Circulation. Geophysical Research Letters, 47, 2020. doi: 10.1029/2019GL086075.